

Quantum theory for electron spin decoherence induced by nuclear spin dynamics in semiconductor quantum computer architectures: Spectral diffusion of localized electron spins in the nuclear solid-state environment

W. M. Witzel

*Condensed Matter Theory Center, Department of Physics,
University of Maryland, College Park, MD 20742-4111*

S. Das Sarma

*Condensed Matter Theory Center, Department of Physics,
University of Maryland, College Park, Maryland 20742-4111*

(Dated: October 30, 2018)

We consider the decoherence of a single localized electron spin due to its coupling to the lattice nuclear spin bath in a semiconductor quantum computer architecture. In the presence of an external magnetic field and at low temperatures, the dominant decoherence mechanism is the spectral diffusion of the electron spin resonance frequency due to the temporally fluctuating random magnetic field associated with the dipolar interaction induced flip-flops of nuclear spin pairs. The electron spin dephasing due to this random magnetic field depends intricately on the quantum dynamics of the nuclear spin bath, making the coupled decoherence problem difficult to solve. We provide a formally exact solution of this non-Markovian quantum decoherence problem which numerically calculates accurate spin decoherence at short times, which is of particular relevance in solid-state spin quantum computer architectures. A quantum cluster expansion method is developed, motivated, and tested for the problem of localized electron spin decoherence due to dipolar fluctuations of lattice nuclear spins. The method is presented with enough generality for possible application to other types of spin decoherence problems. We present numerical results which are in quantitative agreement with electron spin echo measurements in phosphorus doped silicon. We also present spin echo decay results for quantum dots in GaAs which differ qualitatively from that of the phosphorus doped silicon system. Our theoretical results provide the ultimate limit on the spin coherence (at least, as characterized by Hahn spin echo measurements) of localized electrons in semiconductors in the low temperature and the moderate to high magnetic field regime of interest in scalable semiconductor quantum computer architectures.

PACS numbers: 76.30.-v; 03.65.Yz; 03.67.Pp; 76.60.Lz

I. INTRODUCTION

Quantum computation considerations have generated a great deal of recent interest in the old^{1,2,3,4,5,6} problem of electron spin coherence in semiconductors. In particular, a localized electron spin can act as a qubit (i.e., a quantum dynamical two-level system) for quantum information processing in scalable solid-state quantum computer architectures.^{7,8} But using such spin qubits for quantum information processing purposes necessarily requires long spin coherence time, and therefore understanding electron spin decoherence in the solid-state environment becomes a key issue. In this paper, we develop a quantum theory for, what we consider to be, the most important electron spin decoherence mechanism in spin-qubit based semiconductor quantum computer architectures. The spin decoherence mechanism we consider here is the so-called spectral diffusion mechanism, which has a long history,^{1,2,3,4,5,6} and has been much-studied recently^{9,10,11,12,13} in the context of spin qubit decoherence.

To provide a physical background for the theory to be presented in this paper we start by considering a localized electron in a solid, for example, a donor-bound

electron in a semiconductor as in the doped Si:P system. Such a Si:P system is the basis of the Kane quantum computer architecture.⁷ The electron spin could decohere through a number of mechanisms. In particular, spin relaxation would occur via phonon or impurity scattering in the presence of spin-orbit coupling, but these relaxation processes are strongly suppressed in localized systems and can be arbitrarily reduced by lowering the temperature. In the dilute doping regime of interest in quantum computation, where the localized electron spins are well-separated spatially, direct magnetic dipolar interaction between the electrons themselves is not an important dephasing mechanism.¹⁴ Interaction between the electron spin and the nuclear spin bath is therefore the important decoherence mechanism at low temperatures and for localized electron spins. Now we restrict ourselves to a situation in the presence of an external magnetic field (which is the situation of interest to us in this paper) and consider the spin decoherence channels for the localized electron spin interacting with the lattice nuclear spin bath. Since the gyromagnetic ratios (and hence the Zeeman energies) for the electron spin and the nuclear spins are typically a factor of 2000 different (the electron Zeeman energy being larger), hyperfine coupling induced direct spin-flip transitions between

electron and nuclear spins would be impossible at low temperature since phonons would be required for energy conservation.¹⁵ This leaves the indirect spectral diffusion mechanism¹⁸ as the most effective electron spin decoherence mechanism at low temperatures and finite magnetic fields. The spectral diffusion process is associated with the dephasing of the electron spin resonance due to the temporally fluctuating nuclear magnetic field at the localized electron site. These temporal fluctuations cause the electron spin resonance frequency to diffuse in the frequency space, hence the name spectral diffusion. The specific electron spin spectral diffusion process being considered in this work is that arising from the magnetic dipolar interaction induced flip-flop mechanism in nuclear spins. Other local flip-flop mechanisms between nuclei, such as indirect exchange interactions^{20,21,22} (which we will briefly address in this paper in the context of GaAs), may be easily included in our formalism.

Spectral diffusion (SD) is, in principle, not a limiting decoherence process for silicon or germanium based quantum computer architectures because these can, in principle, be fabricated free of nuclear spins using isotopic purification. Unfortunately this is not true for the important class of materials based on III-V compounds, where SD has been shown to play a major role.^{9,14} There is as yet no direct (e.g., GaAs quantum dots) experimental measurement of localized spin dephasing in III-V materials, but such experimental results are anticipated in the near future. Indirect spin echo measurements based on singlet-triplet transitions in coupled GaAs quantum dot systems²³ give T_2 times consistent with our theoretical results.

SD is a theoretically challenging problem because the temporally fluctuating random field causing the electron spin dephasing is a non-Markovian stochastic dynamical variable arising from the complex dipolar quantum dynamics of a large number of interacting nuclear spins. Although SD is an intrinsic dephasing mechanism contributing to the so-called T_2 -type (i.e. “transverse”) spin decoherence in the phenomenological Bloch equation language, the effect of SD on the electron spin dynamics (for example, on the electron spin resonance measurement) cannot be characterized by a simple relaxation (or dephasing) time T_2 associated with a “trivial” e^{-t/T_2} type of temporal loss of coherence. The non-Markovian nuclear spin bath dynamics produces a rather complex electron spin dephasing which cannot be characterized by a single decoherence time (except as a very crude approximation). It is therefore more appropriate to consider SD in the context of a specific experimental situation, and it has been traditional, going back to the seminal pioneering work of Hahn, to study SD in the context of the spin echo decay in pulsed spin resonance measurements.^{1,24} In spin echo measurements, the inhomogeneous broadening effects are suppressed by design, and any amplitude decay in the consecutive pulses arises entirely from the T_2 -dephasing time associated with SD (and, of course, other applicable T_2 -type transverse relaxation processes).

It was realized a long time ago^{1,4} that SD due to the dipolar fluctuations of nuclear spins often dominates the coherence decay in electron spin echo experiments. All available theories to date are based on classical stochastic modeling of the nuclear field, a Markovian theoretical framework which is inevitably phenomenological since it requires an arbitrary choice for the spectrum of nuclear fluctuations. Such a classical Markovian modeling is arguably incompatible with the strict requirements of spin coherence and control in a quantum information device. In addition, recent rapid experimental progress in single spin measurements,²⁵ which in the near future promises sensitive measurements of quantum effects in spin resonance, also warrants a quantum theory of SD. In the current work, we develop a quantum theory of spin echo decay in electron spin resonance experiments due to the SD caused by the dipolar interaction induced flip-flop nuclear spin dynamics. We emphasize that, in contrast to all the earlier theories of SD in the literature, our theory is fully quantum mechanical and incorporates the dipolar nuclear spin flip-flop dynamics microscopically without making any phenomenological statistical (Markovian or otherwise) approximations. To the best of our knowledge, ours is the first fully quantum theory for electron spin SD in solid state systems. A proper description of coupled spin dynamics is rather difficult due to the absence of the usual Wick’s theorem for spin degrees of freedom. In that regard, variations of our method may prove rather useful, since environmental spin baths are ubiquitous in any device exploiting the coherent properties of quantum spin systems.

Our theory produces an accurate quantitative and qualitative prediction of the Hahn echo decay. It was pointed out a long time ago^{4,6,11} that the observed time dependence of these echoes are well fitted to the expression $\exp(-t^2)$, a behavior which can be derived phenomenologically⁴ by assuming Lorentzian Brownian motion for the electron spin Zeeman frequency. In our method this approximate behavior arises naturally from the collective quantum evolution of the dipolar coupled nuclei, without any phenomenological assumption on the dynamics of the environment responsible for decoherence. Our theory reveals that the inclusion of quantum corrections to nuclear spin fluctuation increases the degree of decoherence at lower to intermediate time scales, as is best evidenced from our explanation of the existing factor of 3 discrepancy between the Markovian stochastic theory⁹ and experimental data^{6,10,11} of spin echo decay in phosphorus doped silicon.

The rest of this paper is organized as follows. In Sec. II we provide a brief background for the spectral diffusion process; in Sec. III we formulate the theoretical problem of spectral diffusion in the context of Hahn spin echo decay; in Sec. IV we develop and describe the quantum cluster expansion which is the important theoretical result of our work; in Sec. V we describe dual perturbation theories in terms of a τ -expansion and a dipolar perturbation expansion which together explain the convergence

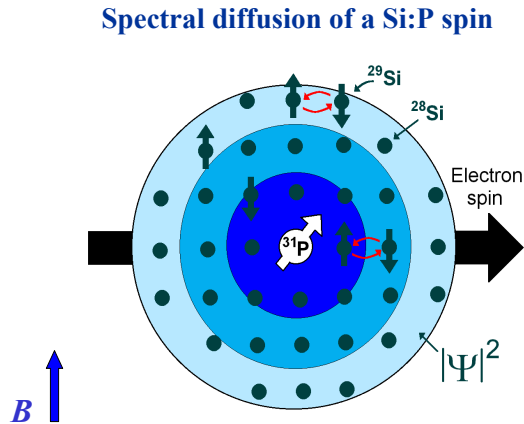


FIG. 1: The electron of a P donor in Si experiences spectral diffusion due to the spin dynamics of the enveloped bath of Si nuclei. Of the naturally occurring isotopes of Si, only ^{29}Si has a net nuclear spin which may contribute to spectral diffusion by flip-flopping with nearby ^{29}Si . Natural Si contains about 5% ^{29}Si or less through isotopic purification. Isotopic purification or nuclear polarization will suppress spectral diffusion.

of our cluster expansion and provide independent verification of its validity; and finally in Sec. VI we apply our theory to obtain numerical results. We conclude in Sec. VII. Five appendixes provide some mathematical details and proofs.

II. BACKGROUND

In systems of interest to us, a qubit is represented by the spin of a localized electron, at low temperature and in a strong external magnetic field, with a wave function that typically envelopes hundreds of thousands of nuclei or more in the surrounding neighborhood of the lattice. Two such examples are the shallow donor electron state in a phosphorus dopant in silicon⁷ and a localized electron in a quantum dot in GaAs.⁸ A schematic²⁶ of the spectral diffusion process in the former is shown in Fig. 1. As discussed in the Introduction, the dominant decoherence method is spectral diffusion (SD) caused by the dynamic evolution of nuclear spins resulting in effective magnetic field fluctuations experienced by the electron. The electron spin couples to nuclear spins via hyperfine interaction in the region in which the electron wave function is appreciable. The nuclear spins couple to each other via dipolar interactions. The large external field suppresses processes that do not conserve electron or nuclear spin polarization in the direction of the magnetic field. Thus the only relevant nuclear processes are flip-flops in which one spin is raised while the other is lowered.

SD is a dephasing decoherence (i.e., a transverse or T_2 -type relaxation) process, affecting only the precession of

the electron spin in the Bloch sphere without changing the electron spin component along the magnetic field. It thus contributes to the energy-conserving T_2 decoherence rather than T_1 decoherence in which energy is exchanged with the bath (Ref. 27 details our definition of T_1 , T_2 , and T_2^*). The T_1 time for these systems at low temperature is known to be much longer than this T_2 time. To analyze this decoherence, we consider an ensemble of spins, initialized in some direction perpendicular to the magnetic field, and observe the decay of the average spin over time. In experiments, many sparse donors or dots serve as the ensemble, and they are initialized by applying a $\pi/2$ -pulse to rotate electron spins polarized along the magnetic field axis into the plane perpendicular to the magnetic field. For the free induction decay (FID), no further pulses are applied and the observed decay is largely due to inhomogeneous broadening which is caused by the difference in the local magnetic field of each electron, causing precession at different rates for different electrons. This will provide what is referred to as the T_2^* decoherence time. At the very least, this inhomogeneous broadening is a result of the random initial distribution of nuclear spin states which gives an uncertainty that scales as \sqrt{N} where N is the effective number of nuclei ($\gtrsim 10^5$) influencing the electron significantly. This decoherence due to inhomogeneous broadening can be eliminated by refocusing methods such as the Hahn echo.²⁴ In such an experiment, a π -pulse, resonant with electron spins, is applied at time $t = \tau$ in the same direction as the original $\pi/2$ pulse and then an echo is observed at $t = 2\tau$. This has the effect of reversing any static local field effects and allows us to obtain the actual SD decoherence (i.e., the T_2 decoherence as opposed to T_2^* decoherence) caused by effective magnetic field fluctuations. This experiment provides a measure of T_2 . The current paper will analyze the Hahn echo experiment. More sophisticated pulses, such as the Carr-Purcell-Meiboom-Gill sequence,²⁸ can yield even longer decoherence times and will be analyzed in future publications.

Previous attempts at analyzing this SD decoherence have been based on quasiclassical stochastic modeling. Herzog and Hahn¹ assigned a phenomenological Gaussian probability distribution function for the Zeeman frequency of the investigated spin without considering the dynamics of the nuclear bath. Later, Klauder and Anderson⁴ used a Lorentzian distribution function instead in order to account for a power law time dependence observed in experiments by Mims and Nassau.³ Zhidomirov and Salikhov⁵ devised a more sophisticated theory, with a wider range of applicability, in which the flip rate of each spin in the bath was characterized by Poisson distributions. Very recently de Sousa and Das Sarma,⁹ in considering spectral diffusion by nuclear spin flip-flops, extended this theory to characterize flip-flop rates of pairs rather than individual spins within a phenomenological model.

In this paper, we present a microscopic theory that is based entirely on the quantum mechanics of the sys-

tem without resorting to phenomenological distribution functions. No Markovian assumption nor any assumption about the form of the solution was used to obtain our results here. Our expansion is entirely based upon a density matrix formulation of the problem which assumes infinite nuclear spin temperature ($T \gg \text{nK}$) and uses an approximate but microscopic Hamiltonian. The problem obviously involves too many nuclear spins to solve directly using exact Hamiltonian diagonalization; however, the cluster expansion method we devise can give successive approximations to the exact solution (convergent for short times, but often out to the tail of the decay such that the full solution is obtained for practical purposes). A short report of our results without any theoretical details has earlier appeared as a Rapid Communication [12]. Our lowest order solution¹² was recently reproduced by Yao *et al.*¹³ using an entirely different approach, thus providing an independent validation of our theoretical approach.

III. FORMULATION OF THE PROBLEM

A. Free evolution Hamiltonian

The free evolution Hamiltonian for the spectral diffusion problem, considering one localized electron spin, \mathbf{S} , and a nuclear spin bath, \mathbf{I}_n , in an external magnetic field B (taken to be along the z direction), is given by

$$\mathcal{H} = \mathcal{H}^{Ze} + \mathcal{H}^{Zn} + \mathcal{H}^A + \mathcal{H}^B, \quad (1)$$

where the first two terms are due to the Zeeman energies of the electron and nuclei respectively, \mathcal{H}^A gives the electron-nuclei coupling, and \mathcal{H}^B contains the internuclear coupling.

The Zeeman energy contributions, arising from the external magnetic field, are given by

$$\mathcal{H}^{Ze} = \gamma_S B S_z, \quad (2)$$

$$\mathcal{H}^{Zn} = -B \sum_n \gamma_n I_{nz}, \quad (3)$$

where γ_S and γ_n are the gyromagnetic ratios of the electron spin and nuclear spins, respectively, and B is the external magnetic field defined to point in the z direction.

The electron-nuclei coupling is given by

$$\mathcal{H}^A = \sum_n A_n (\mathbf{I}_n \cdot \mathbf{S}). \quad (4)$$

A_n gives the magnetic coupling between the electron spin and each nuclear spin. It is dominated by the hyperfine coupling for nuclei that contribute significantly to SD. Since $\gamma_S = 1.76 \times 10^7 (\text{s G})^{-1}$ is typically four orders of magnitude larger than γ_n , flip-flop processes between the electron and a nuclear spin are strongly suppressed at low temperatures (i.e., no phonons) by energy conservation

in a strong magnetic field.¹⁵ This direct hyperfine interaction leads to quantitatively important effects at zero magnetic field,²⁹ but at the moderate or high magnetic fields required for spin resonance measurements it only contributes a small visibility decay.³⁰ We will therefore disregard the nonsecular part of the electron-nuclei coupling, leaving us with

$$\mathcal{H}^A \approx \sum_n A_n I_{nz} S_z, \quad (5)$$

which we will use as the definition for \mathcal{H}^A throughout the rest of this paper.

The internuclear coupling due to the dipolar interaction is given by³¹

$$\mathcal{H}^B = \sum_{n \neq m} \mathcal{H}_{nm}^B, \quad (6)$$

$$\mathcal{H}_{nm}^B = \frac{\gamma_n \gamma_m \hbar}{2} \left[\frac{\mathbf{I}_n \cdot \mathbf{I}_m}{R_{nm}^3} - \frac{3(\mathbf{I}_n \cdot \mathbf{R}_{nm})(\mathbf{I}_m \cdot \mathbf{R}_{nm})}{R_{nm}^5} \right], \quad (7)$$

where \mathbf{R}_{nm} is the vector joining nuclei n and m . This can be expanded into a form containing only operators of the type I_+ , I_- , or I_z .³¹ We will again invoke the energy conservation argument which, because of the strong external magnetic field, allows us to neglect any term that changes the total Zeeman energy of the nuclei. This will leave us with the following secular contribution:

$$\mathcal{H}_{nm}^B \approx b_{nm} (\delta(\gamma_n - \gamma_m) I_{n+} I_{m-} - 2 I_{nz} I_{mz}), \quad (8)$$

$$b_{nm} = -\frac{1}{4} \gamma_n \gamma_m \hbar \frac{1 - 3 \cos^2 \theta_{nm}}{R_{nm}^3}, \quad (9)$$

where θ_{nm} is the angle of \mathbf{R}_{nm} relative to the magnetic field direction. Equation (8) will be used for \mathcal{H}_{nm}^B throughout the rest of this paper. Note that the flip-flop interaction between nuclei with different gyromagnetic ratios is suppressed by Zeeman energy conservation in the same way that the nonsecular part of the dipolar interaction is suppressed. This occurs, for example, in GaAs because the two isotopes of Ga and the one isotope of As that are present have significantly different gyromagnetic ratios. This approximation is applicable if any such differences in γ_n are on the order of $|\gamma_n|$ itself and thus such energy changes would be large compared to other energies of the problem in the large external magnetic field being considered in this work. Giving some typical numbers, $\max(|A_n|) \sim 10^6 \text{ s}^{-1}$, $\max(|b_{nm}|) \sim 10^2 \text{ s}^{-1}$, and for $B = 10 \text{ T}$, $|\gamma_n B| \sim 10^8 \text{ s}^{-1}$ and $|\gamma_S B| \sim 10^{12} \text{ s}^{-1}$. The Zeeman energies are thus much larger than the other energies in the problem. In fact, our model of neglecting terms that change the total Zeeman energy of the nuclei turns out to be reasonably valid for $B > 0.1 \text{ T}$ or so for Si:P or GaAs systems of interest to us. SD is therefore the dominant spin decoherence channel for localized electrons in semiconductors except at zero or very small ($< 0.1 \text{ T}$) magnetic fields.

B. Hahn echo

The Hahn echo experiment consists of preparing the electron spin in a state perpendicular to the magnetic field, allowing free evolution for a time τ , applying an electron spin resonant π -pulse about an axis perpendicular to the magnetic field (for our theoretical purpose, the direction of this axis is not important beyond being perpendicular to the B -field), and then allowing free evolution again for time τ . The echo envelope is the magnitude of the resulting ensemble spin average at time $t = 2\tau$.

Mathematically, the echo envelope is the magnitude of the expectation value of the spin multiplied by 2 for normalization (since the electron has a spin of $1/2$). Because we are only concerned with the component of the spin perpendicular to the magnetic field, it is also the magnitude of the normalized complex in-plane magnetization:

$$v_E(\tau) = 2(\langle S_x \rangle + i\langle S_y \rangle) \quad (10)$$

$$= 2 \operatorname{Tr} \{ (S_x + iS_y) \rho(\tau) \}. \quad (11)$$

The density matrix of the system, $\rho(\tau)$, is given by

$$\rho(\tau) = U(\tau) \rho_0 U^\dagger(\tau), \quad (12)$$

with the evolution operator

$$U(\tau) = e^{-i\mathcal{H}\tau} \sigma_{x,e} e^{-i\mathcal{H}\tau}, \quad (13)$$

where \mathcal{H} is the free evolution Hamiltonian given by Eq. (1). We have arbitrarily chosen the pulse axis to be in the x direction. This pulse is represented by the Pauli matrix, $\sigma_{x,e} = 2S_x$ with the e subscript denoting that it is an electron spin operator.

Our initial density matrix, ρ_0 , will be given by a product state of the electron spin, in a direction perpendicular to the magnetic field, and the nuclear spins in a thermal state:

$$\rho_0 = |\chi_e^0\rangle \langle \chi_e^0| \otimes \frac{e^{-\mathcal{H}^n/k_B T}}{M}, \quad (14)$$

$$|\chi_e^0\rangle = \frac{1}{\sqrt{2}}(|0_e\rangle + e^{i\phi}|1_e\rangle), \quad (15)$$

where $\mathcal{H}^n = \mathcal{H}^{Zn} + \mathcal{H}^B$ and M is its partition function ($M \approx 2^N$ for $T \gg$ nK, where N is the number of nuclear spins). The initial angle of the spin, ϕ , will contribute an irrelevant phase factor to the complex in-plane magnetization. Dropping this irrelevant phase (since we are interested in the magnitude), after a few manipulations, shown in Appendix A, Eq. (11) becomes

$$v_E(\tau) = \frac{1}{M} \operatorname{Tr} \left\{ U_- U_+ e^{-\mathcal{H}^n/k_B T} U_-^\dagger U_+^\dagger \right\}, \quad (16)$$

where

$$U_\pm = e^{-i\mathcal{H}^\pm \tau} \quad (17)$$

are evolution operators under the effective Hamiltonians

$$\mathcal{H}^\pm = \sum_{n \neq m} \mathcal{H}_{nm}^B \pm \frac{1}{2} \sum_n A_n I_{nz}, \quad (18)$$

which describe nuclear evolution under the effect of an electron spin up (\mathcal{H}^+) or down (\mathcal{H}^-) with the external magnetic field dependence now canceled out. Although the U_\pm evolution operators are independent of B , it should be noted that a strong external magnetic field is required to justify the approximations of Eqs. (5) and (8). The trace in Eq. (16) is taken over nuclear spin states only.

For our purposes we only consider high nuclear temperatures ($T \gg$ nK) such that we can make the following approximation:

$$v_E(\tau) = \frac{1}{M} \operatorname{Tr} \left\{ U_- U_+ U_-^\dagger U_+^\dagger \right\}. \quad (19)$$

The high nuclear temperature (and the low electron and phonon temperature) approximation made throughout this work is well-valid in the solid-state quantum computer architectures of our interest, where typical experiments would be carried out around $T \sim 100$ mK which is an extremely high temperature for the nuclear bath dynamics and an extremely low temperature for phonon excitations.

IV. CLUSTER METHOD

Our cluster method provides a strategy to compute the Hahn echo, $v_E(\tau)$ [Eq. (19)], in successive orders of accuracy which may or may not converge for a specific application (naturally the systems reported in this paper do converge, for practical purposes, as we will show). We refer to these successive orders, loosely, as an “expansion” although we do not wish to suggest that corrections are additive (as in familiar expansions such as a Taylor series). In Sec. IV A, we provide a conceptual description of this cluster expansion. Section IV B supplies the mathematical formalism and practical implementation of this expansion.

A. Conceptual cluster expansion

Consider independent, simultaneous nuclear “processes” that may contribute to the decay of the Hahn echo. For example, a process may involve a pair of nuclei flip-flopping [Fig. 2(a)] which results in fluctuations of the effective magnetic field seen by the electron spin, or it may involve three nuclei interdependently [Fig. 2(b)], etc. The dynamics of such a process results from the local coupling between nuclei (with coupling constants $\{b_{nm}\}$), and hyperfine coupling to the electron (with coupling constants $\{A_n\}$). Any number of these processes

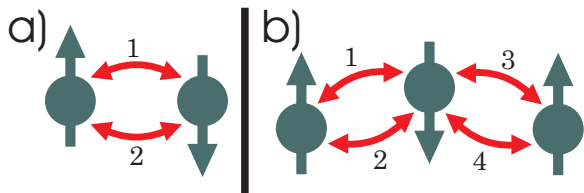


FIG. 2: Some possible nuclear “processes” where the numbered two-sided arrows represent a sequence of flip-flops between pairs of nuclei. (a) depicts a two-nuclei process and (b) depicts a three-nuclei process.

may occur “simultaneously” as long as they involve disjoint sets of nuclei and are thus independent of each other (processes that share a nucleus are not independent and would have to be combined into a larger process).

Using this (not yet well-defined) concept of nuclear processes, the cluster expansion may be described, ideally, as follows. The cluster expansion will include processes that involve a successively increasing number of nuclei. Because an isolated nucleus in our model does not contribute to spectral diffusion, at the lowest nontrivial order we include any simultaneous processes involving two nuclei (pairs). Thus at this lowest order we can involve any number of pair processes together as long as the pairs do not overlap (i.e., involve the same nucleus). At the next order, we will additionally include processes that involve three nuclei. Next, we include four nuclei processes which cannot be decomposed into two pair processes (these would already have been included). To summarize, let us say that the k^{th} order of the expansion will include processes of up to k nuclei.

Because *all* processes involving a given number of nuclei are included at each order of this expansion, and because these processes are independent (proven formally in Sec. IV B and the related appendix), rather than working with individual processes, we can work with contributions due to each given “cluster” of nuclei (for now, simply defined as a set of nuclei); such a “cluster contribution” includes contributions from all of the processes involving all nuclei in that cluster in an interdependent way (i.e., not separable into independent sub-processes). Thus we may say that the k^{th} order of the expansion includes contributions from clusters up to size k . These “contributions” are not necessarily additive in the solution because we must account for simultaneous but independent processes (from disjoint clusters). The idea is simply to include the possibility of interdependent processes involving clusters of successively increasing size.

We deliberately use the word “cluster” to imply proximity between the members of the set of nuclei involved in interdependent processes. In fact, a near neighbor approximation, in which the constituent nuclei of a contributing cluster must be in the same neighborhood, is justified by the $1/\mathbf{R}_{nm}^3$ dependence of the internuclear coupling constant [Eq. (9)]. Consider a near (not necessarily nearest) neighbor approximation with an ad-

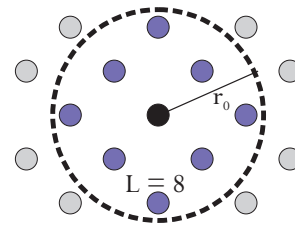


FIG. 3: L is loosely defined as the average number of neighbors in a near neighbor approximation that converges to the exact answer. For example, we can include neighbors up to a distance r_0 away such that increasing this maximum neighbor distance in the near neighbor approximation (where non-neighbor interactions are neglected) does not significantly change the solution.

justable parameter r such that we ignore interactions between nuclei that are a further apart than r . If a near neighbor approximation is applicable, the Hahn echo solution in this approximation (in principle, whether or not it is feasible to compute) will converge with an acceptable level of accuracy at some finite value of r much smaller than the system size. Let us define r_0 to be the value of r in which this acceptable convergence is achieved. Let L be the number of nuclei within a range of r_0 from any nucleus, on average, as shown in Fig. 3. Applying this near neighbor approximation to our cluster expansion, L determines the way in which the number of contributing clusters scales with cluster size. This has important implications for the convergence of the cluster expansion.

To be specific, the convergence of the cluster expansion depends upon two factors. The first is how the number of contributing clusters scales with cluster size (which relates to L as we have already said). The second is how the average contribution of clusters scales with cluster size. Clusters only contribute via interdependent processes; thus the set of nuclei in a contributing cluster must form a connected graph where edges in the graph connect neighbors [Fig. 4(a)]. When counting the number of clusters of a given size, we have N sites to choose from for the first nucleus, but there are only $\mathcal{O}(L)$ possibilities (roughly) for each additional nucleus because it must neighbor one of the previous choices. This simple analysis does not compensate for overcounting due to permuting labels and other such details, but it provides the correct scaling in terms of N and L ; that is, there are $\mathcal{O}(NL^{k-1})$ contributing clusters of size k . Our first scaling factor is then L since the number of clusters as a function of cluster size scales in powers of L . The other scaling factor will rely upon some perturbation theory to describe how cluster contributions themselves scale with an increase in cluster size. Section V will discuss two perturbation theories that may be applicable [for short times, $\tau \ll \max(b_{nm})^{-1}$], but for now we will use λ to represent some perturbation parameter and assume that a cluster contribution of size k will scale as $\mathcal{O}(\lambda^k)$. Thus λ is assigned as the other scaling factor, and we may loosely

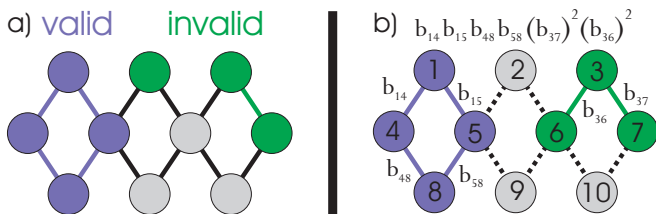


FIG. 4: (Color online) (a) The set of nuclei in a contributing cluster must form a connected graph. Edges represent neighbor connections. The set of blue nuclei on the left form a valid cluster. The set of green nuclei on the upper right are not fully connected so they do *not* form a valid cluster. (b) A set of b_{nm} factors in a term of an expansion of $v_E(\tau)$ determines a set of disjoint clusters (the connected subgraphs formed from b_{nm} edges).

argue that we expect the cluster expansion to converge when $\lambda L \ll 1$ because the total contribution from clusters then decreases as we increase in cluster size. This reasoning will become more rigorous when we go on to explain how we implement this cluster expansion.

B. Mathematically formalized cluster expansion

In Sec. IV A, we gave a rough, conceptual description of our cluster expansion to guide the reader’s intuition and present some basic ideas. At this point, we will develop the rigorous mathematical formalism that relates the idea of simultaneous, independent nuclear processes contributing to the Hahn echo directly to our mathematical expression [Eq. (19)] for the Hahn echo. We will decompose Eq. (19) into a sum of products of cluster contributions. Each cluster contribution will effectively contain the sum of contributions from all processes involving, inseparably (i.e., interdependently), all nuclei in the cluster. Such a decomposition requires that processes involving disjoint sets of nuclei are truly independent and interchangeable. This requirement is met by proving, as we shall, that a cluster contribution is independent of anything outside of the cluster.

These cluster contributions need not be computed by analyzing the possible “processes” involving each set of nuclei. Instead, the decomposition of Eq. (19) into cluster contributions will be used recursively to define these cluster contributions; this is shown in Sec. IV B 1. With these cluster contributions concretely defined, we then discuss, in Sec. IV B 2, how we mathematically define the ideal cluster expansion that we have conceptually described. This ideal expansion is useful for understanding some basic ideas, but in order to practically perform calculations on large systems, some further approximation techniques must be used. This practical implementation of the cluster expansion is explained in Sec. IV B 3.

1. Decomposing into cluster contributions

Consider expanding $v_E(\tau)$ [Eq. (19)] into a sum of products with respect to internuclear coupling, having all b_{nm} constants factorable from each term. For example, such an expansion could be made by Taylor expanding the exponentials of U_{\pm} [Eq. (17)] and then distributing through these sums. Each term in such an infinite expansion has a set of b_{nm} factors which determine a set of involved clusters. In the language of graph theory, the b_{nm} factors may be represented by edges (between nodes n and m); then the clusters are the sets of nuclei in each connected subgraph (each of these being involved in an interdependent process). Figure 4(b) illustrates an example of this. In this way we begin to relate our concept of clusters of interdependent processes to Eq. (19).

Each term in such a sum of products expansion will involve some disjoint set of clusters. Let us assume that processes involving disjoint clusters are truly independent. For a particular cluster, \mathcal{C} , we should then be able to factor out a unique cluster contribution from those terms which involve cluster \mathcal{C} . This is the basis for a decomposition of $v_E(\tau)$ into cluster contributions. It will be useful to generalize this by defining $v_{\mathcal{S}}(\tau)$ to be the solution to the Hahn echo, $v_E(\tau)$ [Eq. (19)], when only including the nuclei in some set \mathcal{S} . We will use $v'_{\mathcal{C}}(\tau)$ to represent the contribution from cluster \mathcal{C} . Appendix B proves that the cluster contributions are independent of each other in a way that allows for the following decomposition of $v_{\mathcal{S}}(\tau)$:

$$\begin{aligned} v_{\mathcal{S}}(\tau) &= \sum_{\substack{\{\mathcal{C}_i\} \text{ disjoint,} \\ \mathcal{C}_i \neq \emptyset, \mathcal{C}_i \subseteq \mathcal{S}}} \prod_i v'_{\mathcal{C}_i}(\tau) \quad (20) \\ &= 1 + \sum_{\substack{\{\mathcal{C}_i\} \neq \emptyset \text{ disjoint,} \\ \mathcal{C}_i \neq \emptyset, \mathcal{C}_i \subseteq \mathcal{S}}} \prod_i v'_{\mathcal{C}_i}(\tau), \quad (21) \end{aligned}$$

where the summation of Eq. (20) is over all possible sets, $\{\mathcal{C}_i\}$, of disjoint nonempty clusters, \mathcal{C}_i , each of which is contained in or equal to \mathcal{S} . In other words, it iterates over all possible ways of dividing any part of \mathcal{S} into disjoint clusters as depicted in Fig. 5. The product is over all clusters in each set. Despite the index, i , the order is irrelevant and permutations do not count as distinct cases. Extracting the trivial $\{\mathcal{C}_i\} = \emptyset$ term yields Eq. (21), shown explicitly to avoid confusion or ambiguity. The unique existence of such a decomposition follows from the fact that any $v'_{\mathcal{C}}(\tau)$ must be well-defined independent of any nuclei outside of \mathcal{C} which is proven in Appendix B.

We can use Eq. (20) itself to obtain an unambiguous expression for any $v'_{\mathcal{C}}(\tau)$. We do this by applying Eq. (20) to the case in which $\mathcal{S} = \mathcal{C}$ and pulling out the term, from the summation, in which $\{\mathcal{C}_i\} = \{\mathcal{C}\}$ leaving only sets in which all $\mathcal{C}_i \neq \mathcal{C}$:

$$v_{\mathcal{C}}(\tau) = v'_{\mathcal{C}}(\tau) + \sum_{\substack{\{\mathcal{C}_i\} \text{ disjoint,} \\ \mathcal{C}_i \neq \emptyset, \mathcal{C}_i \subset \mathcal{C}}} \prod_i v'_{\mathcal{C}_i}(\tau), \quad (22)$$

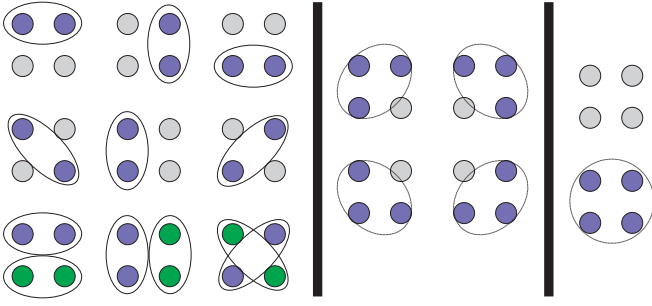


FIG. 5: Set of all possible sets, $\{C_i\}$, of disjoint contributing clusters contained in a set, \mathcal{S} , of four nuclei as an example. Contributing clusters are of size 2 or greater (a single nucleus gives no contribution on its own). The cases on the left involve 2-nuclei, middle ones involve 3-nuclei, and the ones on the right are the trivial cases of $\{C_i\} = \emptyset$ or $\{C_i\} = \{\mathcal{S}\}$. Such possibilities are iterated over in the summation of Eq. (20). Equation (21) removes the $\{C_i\} = \emptyset$ case and Eq. (23) removes the $\{C_i\} = \{\mathcal{S}\} = \{\mathcal{C}\}$ case from their respective summations.

so that

$$v'_C(\tau) = v_C(\tau) - \sum_{\substack{\{C_i\} \text{ disjoint,} \\ C_i \neq \emptyset, C_i \subset C}} \prod_i v'_{C_i}(\tau). \quad (23)$$

Equation (23) provides a recursive definition of a cluster contribution. Starting with the computation of $v_C(\tau)$, which is feasible to calculate directly for small clusters, one must subtract terms that involve multiple independent processes and processes that do not involve all of the nuclei in \mathcal{C} . It is a direct consequence of the decomposition given by Eq. (20).

To ensure that Eq. (23) is well-understood, we show more explicit results for clusters of size one through four. Because a single isolated nucleus cannot contribute to spectral diffusion, $v'_{C_1}(\tau) = v_{C_1}(\tau) - 1 = 0$ when $|C_1| = 1$. It follows that for 2-clusters, $v'_{C_2}(\tau) = v_{C_2}(\tau) - 1$ (with $|C_2| = 2$), having no contributing proper subclusters. For 3-clusters, we must subtract off contributions from contained pairs:

$$v'_{C_3}(\tau) = v_{C_3}(\tau) - 1 - \sum_{\substack{C_2 \subset C_3, \\ |C_2|=2}} v'_{C_2}(\tau). \quad (24)$$

For 4-clusters, we must also subtract off contributions from contained 3-clusters and the products of contributions from contained disjoint pairs:

$$v'_{C_4}(\tau) = v_{C_4}(\tau) - 1 - \sum_{\substack{C_2 \subset C_4, \\ |C_2|=2}} v'_{C_2}(\tau) - \sum_{\substack{C_3 \subset C_4, \\ |C_3|=3}} v'_{C_3}(\tau) - \frac{1}{2} \sum_{\substack{\mathcal{A} \cup \mathcal{B} = C_4, \\ |\mathcal{A}|=|\mathcal{B}|=2}} v'_{\mathcal{A}}(\tau)v'_{\mathcal{B}}(\tau). \quad (25)$$

The factor of one-half in the last term is needed to compensate for the fact that \mathcal{A} and \mathcal{B} may be swapped in the

summation; it is only a consequence of the notation used here (where \mathcal{A} and \mathcal{B} are interchangeable labels).

2. Ideal cluster expansion

We are now able to compute cluster contributions to be used in the evaluation of our cluster expansion. Revising Eq. (20) slightly, we may write the following expression for the ideal cluster expansion up to k^{th} order:

$$v_E^{(k)}(\tau) = \sum_{\substack{\{C_i\} \text{ disjoint,} \\ C_i \neq \emptyset, |C_i| \leq k}} \prod_i v'_{C_i}(\tau). \quad (26)$$

In order to estimate the error of the k^{th} order of the expansion, we can compare it with the $(k+1)^{\text{th}}$ order which must include contributions from $k+1$ sized clusters. One way to convert $v_E^{(k)}(\tau)$ into $v_E^{(k+1)}(\tau)$ is to add additional terms to the sum in which we replace any k -cluster contribution of an existing term with any $(k+1)$ -cluster contribution generated by adding one neighboring nucleus to the original k -cluster. In doing so, a replacement must be made because the original k -cluster becomes disqualified when we introduce the new $(k+1)$ -cluster which contains it (due to the requirement that the clusters be disjoint). This approach will account for all new sets of $\{C_i\}$ containing a $(k+1)$ -cluster (since any $(k+1)$ -cluster can be made by adding a nucleus to a k -cluster); however, cases will be overcounted because many k -clusters can be used to build the same $(k+1)$ -cluster. This is unimportant because our goal now is to estimate the error of $v_E^{(k)}(\tau)$ relative to $v_E^{(k+1)}(\tau)$ and overestimating this error is just as good. Proceeding along these lines, we first separate out the k -cluster contributions:

$$v_E^{(k)}(\tau) = \sum_{\substack{\{C_i, \mathcal{D}_j\} \text{ disjoint,} \\ 0 < |C_i| < k, |\mathcal{D}_j| = k}} \prod_i v'_{C_i}(\tau) \prod_j v'_{\mathcal{D}_j}(\tau). \quad (27)$$

This performs the same summation over sets of disjoint clusters as in Eq. (26) except that we label k -clusters as \mathcal{D}_j and the smaller clusters as C_i . With these k -clusters now set apart, we can estimate the error of $v_E^{(k)}(\tau)$ relative to $v_E^{(k+1)}(\tau)$ by noting that the sum of all $(k+1)$ -cluster contribution replacements of $v'_{\mathcal{D}_j}(\tau)$ are roughly $\mathcal{O}(\lambda L) \times |v'_{\mathcal{D}_j}(\tau)|$. Recall that λ was introduced as a perturbation parameter such that a cluster contribution of size k scales as $\mathcal{O}(\lambda^k)$, and L is the average number of neighbors so that there are, roughly speaking, $\mathcal{O}(L)$ $(k+1)$ -clusters that may be built out of one k -cluster. Thus

$$v_E^{(k+1)}(\tau) = \sum_{\substack{\{C_i, \mathcal{D}_j\} \text{ disjoint,} \\ 0 < |C_i| < k, |\mathcal{D}_j| = k}} \prod_i v'_{C_i}(\tau) \times \prod_j v'_{\mathcal{D}_j}(\tau) [1 + \mathcal{O}(\lambda L)]. \quad (28)$$

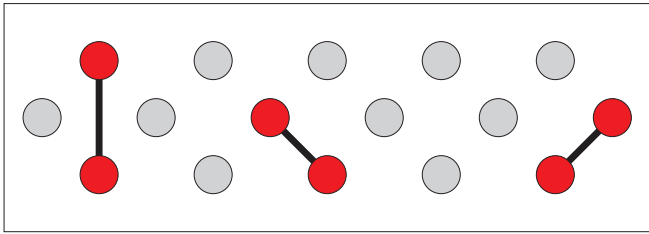


FIG. 6: One possible combination of simultaneously included pair contributions. The red/dark circles are the nuclei whose processes are being considered.

If we explicitly include these $(k+1)$ -clusters, they would have relative corrections of $\mathcal{O}(\lambda L)$ to account for $(k+2)$ -clusters and so forth. This provides a more rigorous argument for our previous assertion that the cluster expansion converges when $\lambda L \ll 1$.

3. Practical implementation of the cluster expansion

Equation (26) directly implements the conceptual cluster expansion as described in Sec. IV A (the inclusion of contributions from all clusters up to size k); however, it is impractical for calculating results in large systems. At the lowest nontrivial order, we would need to sum over all possible products of disjoint pair contributions; for example, Fig. 6 depicts one such combination of disjoint pairs. The number of such possibilities likely grows exponentially with the problem size (we have not bothered to prove this rigorously or look it up, but certainly the scaling with problem size is horrendous). However, we can effectively obtain all possible combinations by making products of the form $\prod_{\mathcal{C}} [1 + v'_{\mathcal{C}}(\tau)]$. Distributing through a given factor yields the possibility of excluding, via the 1 term, or including, via the $v'_{\mathcal{C}}(\tau)$ term, that cluster. Therefore such a product gives the sum of all possible combinations of simultaneous cluster processes (for the clusters included in the product). Unfortunately, this will yield combinations that involve overlapping clusters (that are therefore not independent). These overlapping clusters will introduce an error that, in principle, may be corrected in successive orders of an approximation.

With this approach, the lowest nontrivial order of the expansion may be implemented with

$$v_E^{(2)}(\tau) \approx \prod_{|\mathcal{C}_2|=2} [1 + v'_{\mathcal{C}_2}(\tau)], \quad (29)$$

producing all combinations of pair contributions along with some extraneous terms, such as overlapping pairs as depicted in Fig. 7(b). For a moment, let us disregard these erroneous terms and consider the consequence of this approximation. If we take the logarithm of both sides, we can convert the product on the right-hand side

of Eq. (29) into a convenient sum:

$$\begin{aligned} \ln \left(v_E^{(2)}(\tau) \right) &\approx \sum_{|\mathcal{C}_2|=2} \ln (1 + v'_{\mathcal{C}_2}(\tau)) \quad (30) \\ &\approx \sum_{|\mathcal{C}_2|=2} v'_{\mathcal{C}_2}(\tau) [1 + \mathcal{O}(v'_{\mathcal{C}_2}(\tau))], \quad (31) \end{aligned}$$

where Eq. (31) follows from the Taylor expansion of $\ln(1 + v'_{\mathcal{C}_2}(\tau))$ for $|v'_{\mathcal{C}_2}(\tau)| \ll 1$ which we will shortly justify in a self-consistent way. If we assume that $|v'_{\mathcal{C}_2}(\tau)|$ is small for all (or most) of the \mathcal{C}_2 pairs, then

$$v_E^{(2)}(\tau) \approx \exp[\Sigma_2(\tau)], \quad (32)$$

$$\Sigma_2(\tau) = \sum_{|\mathcal{C}_2|=2} v'_{\mathcal{C}_2}(\tau). \quad (33)$$

It is easy to show, from Eq. (19), that $v_S(\tau)$ is always real and that $-1 \leq v_{\mathcal{C}_2}(\tau) \leq 1$; therefore, $-2 \leq [v'_{\mathcal{C}_2}(\tau) = v_{\mathcal{C}_2}(\tau) - 1] \leq 0$. Because $v'_{\mathcal{C}_2}(\tau = 0) = v_{\mathcal{C}_2}(\tau = 0) - 1 = 0$, $\Sigma_2(\tau = 0) = 0$ and becomes increasingly negative (initially at the very least) as τ is increased. For a large system, we expect $\Sigma_2(\tau)$ to decrease monotonically to a value that is $\mathcal{O}(-N)$ [i.e. $v'_{\mathcal{C}_2}(\tau)$ have become random] so that Eq. (32) exhibits a decay form. The interesting part of the decay occurs when $\Sigma_2(\tau) \gtrsim -1$ so that $v_E^{(2)}(\tau) \gtrsim e^{-1}$. When this is true, the average pair contribution will be, at most, $\mathcal{O}(1/N)$, self-consistently justifying the approximation of Eq. (32) relative to Eq. (31) when N is large (as it is for systems of interest). Increasing τ much beyond this point will bring us to the tail of the decay in which $v_E(\tau) \approx v_E^{(2)}(\tau) \ll 1$. To state this in a physically intuitive way, the decoherence of spectral diffusion is caused by many nuclei collectively such that each potentially flip-flopping nuclear pair contributes only a small amount to the overall dephasing before coherence is completely lost.

For practical purposes [when $v_E(\tau)$ is not terribly small], we thus regard each cluster contribution to be $\mathcal{O}(1/N)$. Now let us discuss the extraneous overlapping pairs of Eq. (29) that we have thus far disregarded. We can now think of these cases, and their corrections, in orders of $1/N$ which increase with the number of overlapping clusters. The lowest order correction will therefore remove cases of two pairs that overlap with each other. For any given pair, there are $\mathcal{O}(L)$ pairs that can overlap with it, each of which has a contribution of $\mathcal{O}(1/N)$ as discussed above. Therefore in estimating the error of Eq. (29) we may write

$$v_E^{(2)}(\tau) = \prod_{|\mathcal{C}_2|=2} \left(1 + v'_{\mathcal{C}_2}(\tau) \left[1 + \mathcal{O}\left(\frac{L}{N}\right) \right] \right). \quad (34)$$

Carrying this error over to Eq. (32) and including its inherent $\mathcal{O}(1/N)$ error, we have

$$v_E^{(2)}(\tau) = \exp \left(\Sigma_2(\tau) \left[1 + \mathcal{O}\left(\frac{1+L}{N}\right) \right] \right). \quad (35)$$

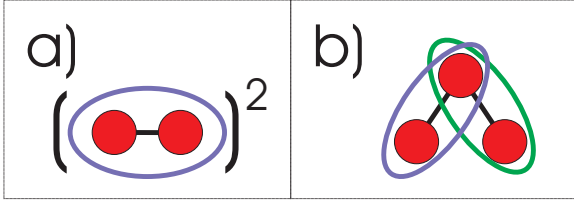


FIG. 7: The practical implementation of the cluster expansion approximates the ideal cluster expansion up to errors resulting from overlapping pairs. At the lowest order, such errors involve overlapping pairs. (a) A single pair multiplied by itself (i.e., a pair overlapping itself) and (b) two pairs overlapping by sharing a nucleus.

Because a cluster contribution scales in orders of λ as we increase the cluster size, this approach may be used for higher order cluster contributions provided that $\lambda \ll N$ (typically, $\lambda \ll 1$ where the cluster expansion is applicable). Taking either $\lambda \ll 1$ or $\lambda \sim 1$, we may write, as an extension of the above approach to higher orders,

$$\ln \left(v_E^{(k)}(\tau) \right) = \sum_{j=2}^k \Sigma_j(\tau) \left[1 + \mathcal{O} \left(\frac{1+L}{N} \right) \right], \quad (36)$$

$$\Sigma_j(\tau) = \sum_{|C|=j} v'_C(\tau). \quad (37)$$

Note that $\Sigma_k(\tau) \sim \Sigma_{k-1}(\tau) \times \mathcal{O}(\lambda L)$, since there are roughly $\mathcal{O}(L)$ times as many k -clusters as $(k-1)$ -clusters and on average each k -cluster contribution, by the definition of λ , is $\mathcal{O}(\lambda)$ times that of the average $(k-1)$ -cluster. With this in mind, we see that, under the cluster expansion, $\ln(v_E(\tau))$ is effectively expanded, additively, in powers of (λL) .

In addition to the expansion in cluster size, we may also successively correct for the $\mathcal{O}(1/N)$ errors of overlapping clusters. This is done by starting with the smallest number of overlapping clusters of the smallest sizes; that is, start with the case of two overlapping pairs (Fig. 7). Each additional cluster included in the set of overlapping clusters being considered will multiply $\mathcal{O}(1/N)$ to the correction, and each additional nucleus added to any cluster will multiply $\mathcal{O}(\lambda L)$ to the correction. For our purposes, we will only consider the correction for two overlapping pairs as a check to verify that the approximation made in Eq. (36) is valid.

There are two cases to consider for this lowest order correction of overlapping clusters: the same pair multiplied by itself [Fig. 7(a)] which was introduced by the approximation of Eq. (31), and two different pairs that overlap [Fig. 7(b)] which originates from Eq. (29). These cases are, respectively, eliminated, to lowest order (two pairs and only two pairs that overlap), by adding the

following to Eq. (36):

$$\Sigma_2^*(\tau) = -\frac{1}{2} \sum_{|C_2|=2} [v'_{C_2}(\tau)]^2, \quad (38)$$

$$\Sigma_3^*(\tau) = -\frac{1}{2} \sum_{\substack{|A \cup B|=3, \\ |A|=|B|=2}} v'_A(\tau) v'_B(\tau), \quad (39)$$

so that

$$\ln \left(v_E^{(k)}(\tau) \right) = \Sigma_2(\tau) + \Sigma_2^*(\tau) + \Sigma_3^*(\tau) + \sum_{j=3}^k \Sigma_j(\tau) \left[1 + \mathcal{O} \left(\frac{1+L}{N} \right) \right]. \quad (40)$$

Exponentiating Eq. (40) then expanding and distributing this exponential into a sum of products form will yield the sum of all products of disjoint cluster contributions, as in Eq. (26), plus extraneous terms of overlapping clusters. However, all cases of only two pairs overlapping with each other (including a pair multiplied by itself) will be removed as a result adding in $\Sigma_2^*(\tau)$ and $\Sigma_3^*(\tau)$. There will remain higher order errors with more than two overlapping clusters or overlapping clusters larger than pairs; in fact, additional higher order errors are introduced by the $\Sigma_2^*(\tau)$ and $\Sigma_3^*(\tau)$ corrections itself. For this reason, it is difficult to derive higher order corrections (you must correct errors introduced by lower order corrections). We can, however, regard this lowest order correction as an estimate of the error caused by these extraneous overlapping clusters:

$$\ln \left(v_E^{(k)}(\tau) \right) = \sum_{j=2}^k \Sigma_j(\tau) + \mathcal{O}(\Sigma^*(\tau)), \quad (41)$$

$$\Sigma^*(\tau) = \Sigma_2^*(\tau) + \Sigma_3^*(\tau). \quad (42)$$

Note that $\Sigma_2^*(\tau)$ and $\Sigma_3^*(\tau)$ are both ≤ 0 and therefore add constructively (otherwise we would want to take absolute values in order to estimate the error conservatively). Fortunately, calculations of $\Sigma^*(\tau)$ indicate that it is a minor correction for practical purposes. Such calculations verify the argument that these are $\mathcal{O}(1/N)$ errors [at least for practical values of τ for which $v_E(\tau) \gtrsim e^{-1}$].

C. Cluster expansion in summary

The cluster expansion method that we have developed in this section is very powerful and very general. The disjoint cluster decomposition [Eq. (20)] could be used to take the trace of any evolution operators described by Hamiltonians with pairwise (or even higher order) interactions. This decomposition may then be used to form an expansion [Eq. (26)] that converges when the sum of cluster contributions decreases with cluster size (i.e., $\lambda L \ll 1$). In order to practically compute this expansion for a large system, we need to use approximations

such as Eq. (34) or Eq. (36) which have the additional requirement that each cluster contribution be small, e.g., $\mathcal{O}(1/N)$, so that extraneous overlapping clusters arising from these approximations are small. This is, in principle, a formally exact, systematic expansion and its convergence may be tested by comparing $\Sigma_j(\tau)$ for at least $j = 2, 3$, and 4 as well as $\Sigma^*(\tau)$. It is important to compute $\Sigma_4(\tau)$ as well as $\Sigma_3(\tau)$ because a symmetry of the problem eliminates all odd orders of λ as we will show for both perturbation theories in Sec. V; therefore, 3 cluster contributions are actually $\mathcal{O}(\lambda^4)$.

We conclude this section by remarking that, besides being elegant and useful for understanding the expansion, the natural logarithm form of the Hahn echo given by Eq. (41) has the advantage that it is convenient to compute $\Sigma_j(\tau)$ and $\Sigma^*(\tau)$ using Monte Carlo techniques. Rather than computing the full sum, randomly selected terms may be sampled and averaged in order to obtain an estimate for each sum. This can save a lot of computation time and makes this method powerful for large, complicated systems.

V. DUAL PERTURBATION THEORIES

The convergence of the cluster expansion, described in the previous section, depends upon how cluster contributions scale with cluster size. In that section, we surmized that a perturbation theory could be invoked such that cluster contributions scale with cluster size in orders of some perturbation parameter, λ ; that is, the contribution of a cluster of size k is $\mathcal{O}(\lambda^k)$. In this way, the cluster expansion relies upon an underlying perturbation theory to justify or explain its convergence. Alternatively, one may regard the cluster expansion as a means to extend convergence of a perturbative expansion to large systems (i.e., even when $N \gg \lambda$). In any case, in order to form a connection between a perturbation theory and the cluster expansion, the contribution of a cluster of size k must be shown to have a minimum perturbative order of λ^k (i.e., lower orders cancel out). In this section, we present two such perturbation theories which are applicable in complementary regimes (and thus, “dual”).

A. Two theories in complementary regimes

Although otherwise complementary, both perturbation theories require that $\tau \ll \max(b_{nm})^{-1}$. However, in problems we have considered $\tau_D \ll \max(b_{nm})^{-1}$ where τ_D is the decay time, and therefore this constraint has no practical consequence. The first perturbation theory we will present is an expansion in orders of τ . For this theory, we can effectively assign $\lambda = \max(b_{nm})\tau$ as the perturbation parameter used in Sec. IV. It is apparent that $\tau \ll \max(b_{nm})^{-1}$ for λ to be small. Besides this requirement, we will see that this perturbative expansion is generally convergent in the regime in which

$|A_n - A_m| \ll b_{nm}$. The second perturbation theory, which we call the dipolar perturbation technique, will treat \mathcal{H}^B of Eq. (8) as a perturbation to the free evolution Hamiltonian. For this theory, $\lambda \sim b_{nm}/|A_n - A_m|$ and is therefore convergent in the opposite regime as the τ -expansion with respect to $|A_n - A_m|$ versus b_{nm} ; that is, $b_{nm} \ll |A_n - A_m|$.

For convenience, we define

$$c_{nm} = \frac{A_n - A_m}{4b_{nm}}, \quad (43)$$

so that the τ -expansion perturbation theory is said to be applicable in the $c_{nm} \ll 1$ regime while the dipolar perturbation is applicable in the $c_{nm} \gg 1$ regime. The factor of 4 in Eq. (43) really only makes sense in the context of spin-1/2 nuclei, but it is irrelevant for the current discussion. Nuclei near the donor or center of the dot, where the electron wave function is strongest so that hyperfine coupling dominates the internuclear coupling [$\max(A_n)/\max(b_{nm}) \sim 10^3$], can typically be classified in the $c_{nm} \gg 1$ regime. Nuclei far from the donor or center of the dot can typically be classified in the opposite regime. A consequence of our perturbative theories is that the extreme cases will give negligible contributions (i.e., there is a “frozen” core where nuclear flip-flops are suppressed by the strong hyperfine coupling, and the electron’s interactions with distant nuclei are too weak to be of consequence). In fact, it is arguable that clusters of the $c_{nm} \sim 1$ regime give the strongest contributions which seems to contradict our supposition that either of these perturbation theories are applicable. However, time plays a role that shifts the balance to the $c_{nm} \gtrsim 1$ side enough to make the dipolar perturbation theory particularly applicable in a way that causes the cluster expansion to converge. This is because the $c_{nm} > 1$ regime implies larger energy scales (with strong hyperfine coupling than the converse) which causes such cluster contributions to operate on shorter time scales and dominate the Hahn echo decay. We would not be satisfied with the face value of this argument, but we have performed a number of numerical calculations that support this conclusion. In particular, we have compared the cluster expansion performed in two ways: one in which cluster contributions are computed exactly, and the other in which these contributions are approximated by dipolar perturbation theory in the lowest order. In order to give convergent results for the latter calculation, a lower bound c_{nm} cutoff must be imposed. However, for a broad range of c_{nm} cutoff values, the two calculations agree very well. This implies that dipolar perturbation theory completely accounts for the Hahn echo decay. The main importance of the τ -expansion perturbation theory is to justify the c_{nm} cutoff by the argument that $c_{nm} \ll 1$ clusters are negligible (although it will have other purposes as we discuss shortly).

We emphasize that the convergence of the cluster expansion is ultimately proven by performing the calculations and comparing the different orders of the expansion

(as we do). The dual perturbation theories serve to explain this convergence.

B. Expansion in τ

Before we devised the cluster method of solving the spectral diffusion problem, we attempted to obtain a solution, at short times, by performing an expansion in τ directly. This met with failure by not converging (for the Si:P system which we tested) even at very short times. We now understand that the reason for the failure of the direct τ -expansion is a combination of the large system size and the difference in the energy (time) scales of the hyperfine coupling and dipolar coupling. In the context of the cluster expansion, however, a perturbation in orders of τ can be applicable. The cluster method deals with large systems correctly and can allow underlying perturbation theories to exhibit themselves without being drowned out by a large $N \gg \lambda^{-1}$.

In Sec. VB1, we will describe the techniques that we developed in order to analyze and compute this τ -expansion. These techniques are shown (in Appendices) as they may be adapted to other problems for which they are more suitable. In Sec. VB2, we show that, in the regime in which the expansion is convergent for small clusters, this provides an underlying perturbation theory to justify the convergence of the cluster expansion (i.e., providing the λ used in Sec. IV). Because of the difference in the energy (time) scales of the hyperfine coupling and dipolar coupling, this perturbation theory is not as relevant as the dipolar perturbation described in Sec. VC; however, we will see that consequences of the τ -expansion are exhibited in GaAs systems (Sec. VIB). Also, Fig. 13 of section VI, provides independent verification of the cluster expansion by using this expansion directly (not in the context of the cluster expansion) for an artificial system in which it is applicable.

1. Algebraic expansion

An expansion in τ is performed by expanding the exponentials of $U_{\pm}(\tau)$ [Eq. (17)] in Eq. (19) and collecting all distributed terms of the desired order in τ . One can additionally expand $e^{-\mathcal{H}^n/k_B T}$, from Eq. (16), in powers of T^{-1} but in the remaining discussion we will be taking the $T \rightarrow \infty$ limit. We developed a symbolic manipulation computer program that gives an exact algebraic expression for any expansion order (although computation time limits the expansions that are feasible). The program uses its own algebraic manipulation library created precisely for this purpose. Appendix C describes the procedure used by the program to obtain this expression.

The computer program's results for $I = 1/2$ were compared to direct hand calculations (as a check) for up to sixth order in τ . Actually, odd orders can be shown to be zero since the result must be real and τ is always ac-

companied by a factor of i . The result is more compact when put in terms of c_{nm} as defined by Eq. (43). In this form the result is

$$v_E(\tau) = 1 - D_4\tau^4 - D_6\tau^6 + \mathcal{O}(\tau^8), \quad (44)$$

$$D_4 = 4c_{nm}^2 b_{nm}^4, \quad (45)$$

$$-\frac{3}{4}D_6 = c_{nm}^4 b_{nm}^6 + c_{nm}^2 b_{nm}^6 + c_{nm}^2 b_{nm}^4 (b_{nk} - b_{mk})^2 + c_{nm} c_{nk} b_{nm}^2 b_{nk}^2 [b_{nk} (b_{nm} + b_{mk}) + b_{mk}^2], \quad (46)$$

where distinct summation over indices is implied for each term. Written in this form, we can surmise that the τ expansion gives convergence for $\max(b_{nm})\tau \ll 1$ in the regime in which most pairs satisfy $c_{nm} \ll 1$. As indicated above, typical spectral diffusion problems have many pairs that satisfy $c_{nm} \gg 1$ instead.

This program has computed algebraic expressions up to $\mathcal{O}(\tau^{10})$ for both $I = 1/2$ and $I = 3/2$. In the $I = 1/2$ case, there are 111 eighth order terms, and 1200 tenth order terms. Terms of order τ^8 have up to four distinct nuclear index labels; terms of order τ^{10} have up to five distinct nuclear index labels. The trend that the number of distinct nuclear indices is half the order of τ will be used in Sec. VB2 to relate the tau expansion to the cluster expansion.

After computing these algebraic expressions, there is an additional challenge of efficiently computing the coefficients of τ from these expressions for specific values of A_n and b_{nm} in order to obtain results such as the τ -expansion plots of Fig. 13. Appendix D describes how this is done.

2. Relating the tau-expansion to clusters

The trend seen above is that the maximum number of distinct nuclear index labels is half of the order of τ . This provides a connection to the cluster expansion. By definition, a cluster contribution must involve all of the nuclei in that cluster. The number of distinct nuclear indices for a cluster contribution is thus equal to the cluster size. Therefore, clusters of size 2 are, at a minimum, fourth order in τ ; clusters of size 3 are $\mathcal{O}(\tau^6)$, etc. Even if we cannot prove that this trend continues beyond $\mathcal{O}(\tau^{10})$ we know that clusters of size greater or equal to 5 are at least $\mathcal{O}(\tau^{10})$. This is a key formal connection between the τ -expansion and the cluster expansion.

We can therefore relate orders of λ used in Sec. IV to orders of τ (up to 5-clusters at least). As long as the τ expansion is convergent for small N , the cluster expansion can extend its convergence for large N . As discussed above, this convergence in τ occurs for $\max(b_{nm})\tau \ll 1$ in the regime in which most pairs satisfy $c_{nm} \ll 1$. We also observed, from the argument that $v_E(\tau)$ must be real, that no odd orders of τ are present. Therefore, as discussed in Sec. IV, the next order of the cluster ex-

pansion beyond pairs should include 3-clusters and 4-clusters.

C. Dipolar perturbation expansion

An expansion in τ is not well-suited, on its own, to practical problems of interest due to the many nuclear pairs satisfying $c_{nm} \gg 1$ [defined in Eq. (43)]. However, in the regime in which $c_{nm} \gg 1$, a nondegenerate perturbation expansion in orders of b_{nm} is applicable. We introduce a bookkeeping parameter λ (which we will later relate to the λ used in Sec. IV, making a formal connection to the cluster expansion) such that $\pm \mathcal{H}^\pm = \mathcal{H}^0 \pm \lambda \mathcal{H}'$. Here the unperturbed Hamiltonian, $\mathcal{H}^0 = \frac{1}{2} \sum_n A_n I_{nz}$, is diagonal in the nuclear spin z -basis, while $\mathcal{H}' = \frac{1}{\lambda} \mathcal{H}^B$ is the dipolar interaction rescaled to have the same magnitude as \mathcal{H}^0 . We note that λ here is a purely formal artifice to define a perturbation expansion using standard perturbation theory in quantum mechanics (and later adapted to the cluster expansion of Sec. IV in order to ensure convergence for large systems).

1. Perturbed Hamiltonian

Using standard perturbation theory in quantum mechanics, we have the following recursive definitions for the eigenvectors and eigenvalues of \mathcal{H}^\pm :

$$|k_\pm\rangle = |k^0\rangle \pm \lambda \sum_{l \neq k} |l^0\rangle \times \quad (47)$$

$$\frac{\langle l^0 | \mathcal{H}' | k_\pm \rangle - \langle l^0 | k_\pm \rangle \langle k^0 | \mathcal{H}' | k_\pm \rangle}{E_k^{(0)} - E_l^{(0)}},$$

$$E_k^\pm = E_k^{(0)} \pm \lambda \langle k^0 | \mathcal{H}' | k_\pm \rangle, \quad (48)$$

$$E_k^{(0)} = \frac{1}{2} \sum_n A_n \langle k^0 | I_{nz} | k^0 \rangle \quad (49)$$

with the normalization convention that

$$\langle k^0 | k \rangle = \langle k^0 | k^0 \rangle = 1. \quad (50)$$

Now we have

$$\mathcal{H}^\pm = \pm \sum_k E_k^\pm \frac{|k_\pm\rangle \langle k_\pm|}{\langle k_\pm | k_\pm \rangle}, \quad (51)$$

where the summation is over all possible states. From Eq. (17),

$$U_\pm(\tau) = \sum_k \frac{|k_\pm\rangle \langle k_\pm|}{\langle k_\pm | k_\pm \rangle} e^{\mp i E_k^\pm \tau}. \quad (52)$$

Plugging this into Eq. (19) we have

$$v_E(\tau) = \sum_{i,j,k,l} \frac{C_{ijkl}}{M} \exp^{-i\omega_{ijkl}\tau}, \quad (53)$$

$$C_{ijkl} = \frac{F_{ijkl}}{D_{ijkl}}, \quad (54)$$

$$F_{ijkl} = \langle l_- | i_+ \rangle \langle i_+ | j_- \rangle \langle j_- | k_+ \rangle \langle k_+ | l_- \rangle, \quad (55)$$

$$D_{ijkl} = \langle i_+ | i_+ \rangle \langle j_- | j_- \rangle \langle k_+ | k_+ \rangle \langle l_- | l_- \rangle, \quad (56)$$

$$\omega_{ijkl} = \omega_{ijkl}^{(0)} + \lambda \omega'_{ijkl}, \quad (57)$$

$$\omega_{ijkl}^{(0)} = E_i^0 - E_j^0 - E_k^0 + E_l^0, \quad (58)$$

$$\omega'_{ijkl} = \langle i^0 | \mathcal{H}' | i_+ \rangle - \langle j^0 | \mathcal{H}' | j_- \rangle - \langle k^0 | \mathcal{H}' | k_+ \rangle + \langle l^0 | \mathcal{H}' | l_- \rangle. \quad (59)$$

We note that C_{ijkl} and ω'_{ijkl} can be expanded in orders of $\lambda \sim c_{nm}^{-1}$.

2. Relating the dipolar perturbation expansion to clusters

In order to show that the dipolar perturbation expansion can be used as an underlying perturbation theory for the cluster expansion (i.e., to supply the λ of Sec. IV), we need to show that for a given term in the λ expansion of Eq. (53), there are at least as many orders of λ as there are nuclei involved (cluster size). In Appendix E, we show this to be effectively the case in the $\max(b_{nm})\tau \ll 1$ limit.

One further point is that $v_E(\tau)$ is an even function of λ . This is seen by noting that under the transformation $\lambda \rightarrow -\lambda$ we have $U_\pm \leftrightarrow U_\mp^\dagger$ and therefore

$$v_E(\tau) = \frac{1}{M} \left| \text{Tr} \left\{ U_- U_+ U_-^\dagger U_+^\dagger \right\} \right| \quad (60)$$

$$\rightarrow \frac{1}{M} \left| \text{Tr} \left\{ U_+^\dagger U_-^\dagger U_+ U_- \right\} \right| = v_E(\tau). \quad (61)$$

This is true because there is a symmetry between ‘‘up’’ and ‘‘down’’; that is, $U_- \leftrightarrow U_+$ is symmetric within the trace operation because $I_{nz} \rightarrow -I_{nz} \forall n$ is symmetric within the trace operation. A consideration of finite nuclear temperatures would break this symmetry, but in our infinite nuclear temperature approximation there will be no odd orders of λ . Therefore, as discussed in Sec. IV, the next order of the cluster expansion beyond pairs should include 3-clusters and 4-clusters. This was shown to be necessary in Sec. VB2 when relating cluster sizes to orders of τ , and it is also true here when relating cluster sizes to orders of the dipolar perturbation expansion.

VI. CALCULATIONS AND RESULTS

The information (i.e., the input) necessary to calculate the spectral diffusion Hahn echo decay, given in Eq. (19) and approximated in the cluster expansion by Eq. (41),

are the A_n , b_{nm} , and I_n (nuclear spin magnitude) values. The internuclear dipolar coupling for b_{nm} is given by Eq. (9). For A_n we use⁹

$$A_n = \frac{8\pi}{3}\gamma_S\gamma_I\hbar|\Psi(\mathbf{R}_n)|^2 - \gamma_S\gamma_I\hbar\frac{1-3\cos^2\theta_n}{|\mathbf{R}_n|}\Theta(|\mathbf{R}_n|-r_0), \quad (62)$$

The first term of Eq. (62) is the hyperfine coupling of the n^{th} nucleus to the electron, while the second term is its dipolar coupling to the electron with r_0 being the effective range of the wave function. \mathbf{R}_n is the position of the n^{th} nucleus relative to the center of the electron wave function and θ_n is its angle relative to the magnetic field direction. While both of these terms were included in our calculations, the dipolar contribution of A_n proves to be negligible for the semiconductor spin quantum computer architectures.

A. Phosphorus donor in silicon

Our first application is to consider the Hahn echo decay of the electron spin of a phosphorus donor in natural silicon.^{6,9,11} Here $\Psi(\mathbf{R}_n)$ is the Kohn-Luttinger wave function of a phosphorus donor impurity in silicon, as described in Ref. 9. Using this in Eq. (62), we have⁹

$$A_n = \frac{16\pi}{9}\gamma_S\gamma_I^{Si}\hbar\eta[F_1(\mathbf{R}_n)\cos(k_0X_n) + F_3(\mathbf{R}_n)\cos(k_0Y_n) + F_5(\mathbf{R}_n)\cos(k_0Z_n)]^2 - \gamma_S\gamma_I^{Si}\hbar\frac{1-3\cos^2\theta_n}{|\mathbf{R}_n|}\Theta(|\mathbf{R}_n|-na), \quad (63)$$

$$F_{1,2}(\mathbf{r}) = \frac{\exp\left[-\sqrt{\frac{x^2}{(nb)^2} + \frac{y^2+z^2}{(na)^2}}\right]}{\sqrt{\pi(na)^2(nb)}}, \quad (64)$$

with $\gamma_S = 1.76 \times 10^7 (\text{s G})^{-1}$, $\gamma_I^{Si} = 5.31 \times 10^3 (\text{s G})^{-1}$, $n = 0.81$, $a = 25.09 \text{ \AA}$, $b = 14.43 \text{ \AA}$, $\eta = 186$, $k_0 = (0.85)2\pi/a_{Si}$, and $a_{Si} = 5.43 \text{ \AA}$. The Si nuclei are located on a diamond lattice.³² The central ^{31}P nuclear spin does not contribute to spectral diffusion because its hyperfine energy is significantly larger than any of its neighbors, suppressing the spin flips by energy conservation.

In a natural sample of silicon, only a small fraction $f = 4.67\%$ of lattice sites have nonzero nuclear spin. These are the spin-1/2 ^{29}Si isotopes, therefore $I_n = 1/2$ for all contributing nuclei. We will use $\langle \Sigma_k(\tau) \rangle$ and $\langle \Sigma_k^*(\tau) \rangle$ to denote $\Sigma_k(\tau)$ and $\Sigma_k^*(\tau)$ averaged, respectively, over isotopic configurations with a fraction, f , of ^{29}Si . We will also use the convention that $\Sigma_k(\tau)$ and $\Sigma_k^*(\tau)$ without these angle brackets gives the $f = 100\%$ result. Thus

$$\langle \Sigma_k(\tau) \rangle = f^k \Sigma_k(\tau), \quad (65)$$

$$\langle \Sigma_k^*(\tau) \rangle = f^k \Sigma_k^*(\tau), \quad (66)$$

where $\Sigma_k(\tau)$, $\Sigma_2^*(\tau)$, and $\Sigma_3^*(\tau)$ are given by Eqs. (37), (38), and (39), respectively, taking all nuclei to be ^{29}Si .

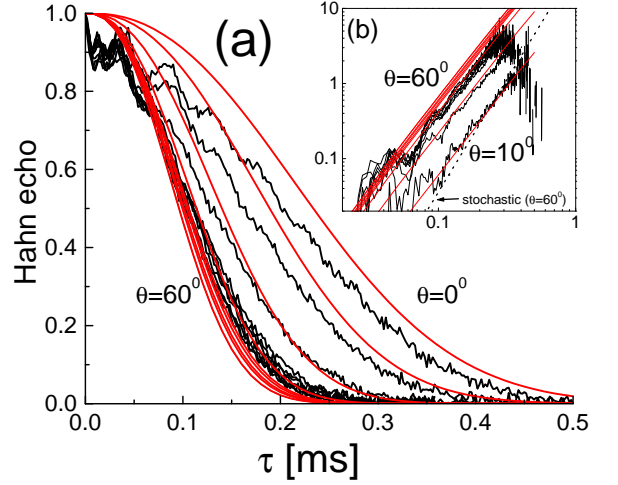


FIG. 8: Hahn echo decay $v_E(\tau, \theta)$ of a phosphorus donor electron spin in silicon due to the dipolar nuclear spin bath dynamics. (a) Theory (solid lines) and experiment (Ref. 10) is shown for several orientation angles of the magnetic field with respect to the crystal lattice, ranging from the [100] to the [110] direction ($\theta = 0, 10, 20, \dots, 90$). (b) Here we plot $-\ln v_E(\tau, \theta) + \ln v_E(\tau, \theta = 0)$, allowing for the removal of any decoherence mechanism which is independent of θ . The qualitative and quantitative agreement between theory and experiment is remarkable, in contrast to the stochastic approach (dashed).

The fact that only a fraction, f , of these nuclei contribute to the diffusion is accounted for by the f^k factors in Eqs. (65) and (66) because f^k is the probability that all nuclei in a cluster of size k have nonzero spin.

For the spin-1/2 nuclei that contribute to spectral diffusion in natural silicon, we can write the following analytical solution for pairs (2-clusters) using Eq. (19):

$$v_{nm}(\tau) = 1 + v'_{nm}(\tau) = 1 - \frac{c_{nm}^2}{(1 + c_{nm}^2)^2} [\cos(\omega_{nm}\tau) - 1]^2, \quad (67)$$

$$\omega_{nm} = 2b_{nm}\sqrt{1 + c_{nm}^2}, \quad (68)$$

where c_{nm} is given by Eq. (43).

Our numerical calculations of Hahn echo decay in the lowest order of the cluster expansion, $v_E^{(2)}(\tau) = \exp(\langle \Sigma_2(\tau) \rangle)$ using Eqs. (65), (37), and (67), are shown for several magnetic field orientation angles in Fig. 8(a) with a direct quantitative comparison to the experiment.¹⁰ The dipolar coupling [Eq. (9)] contains an important anisotropy with respect to the θ_{nm} angle formed between the applied magnetic field and the bond vector linking the two spins (\mathbf{R}_{nm}). This property leads to a strong dependence of spin echo decay when the sample is rotated with respect to the applied B field direction. The experimental data is taken for bulk natural silicon with phosphorus doping concentration equal to $2 \times 10^{15} \text{ cm}^{-3}$ [10]. The high concentration of phosphorus donors leads to an additional decoherence channel arising

from the direct spin-spin coupling between the electron spins that contribute to the echo. This contribution can be shown to add a multiplicative factor $\exp(-\tau/1 \text{ ms})$ to the Hahn echo.³³ Because this contribution is independent of the orientation angle, we can factor it out by subtracting the $\theta = 0$ contribution from the logarithm of the experimental data taken at angle θ . The result is shown in Fig. 8(b) (log-log scale). Our theory seems to explain the time dependence of the experimentally observed echo quite well. This result is to be compared with the recent stochastic theory of Ref. 9 [Dashed line in Fig. 8(b) shows the stochastic calculation for $\theta = 60^\circ$]. Although the stochastic theory yields roughly correct coherence times in order of magnitude, it fails qualitatively in explaining the time dependence [that is, the shape of the decay as can be seen from the incorrect slope of the stochastic calculation in the log-log plot of Fig. 8(b)]. The present method is able to incorporate all these features within a fully microscopic framework, obtaining both qualitative and quantitative agreement with experiment.

An important issue in the context of quantum information processing is the behavior of spin coherence at the shortest time scales. The experimental data¹⁰ in Fig. 8 reveals several oscillatory features which are not explained by our current method. These are echo modulations arising from the anisotropic hyperfine coupling omitted in Eq. (5).¹¹ This effect can be substantially reduced by going to higher magnetic fields. (In a quantum computer $B \sim 9$ Tesla will probably be required in order to avoid loss of fidelity due to echo modulation.³⁴) On the other hand, spectral diffusion itself is essentially independent of magnetic field even to extremely high magnetic field values ($B \sim 10$ Tesla). The echo modulation effect is expected to be absent in III-V materials,³⁵ hence our theory allows the study of spin coherence at time scales of great importance for quantum information purposes, i.e., very short time scales, as long as echo modulation effects are quantitatively unimportant.

Isotopic purification can reduce the value of f (fraction of ²⁹Si nuclei). Figure 9 contains information that is useful for understanding how the Hahn echo curves change as f is changed (i.e., lowered via isotopic purification). In a log-log plot, $\ln(v_E(\tau)) \approx \langle \Sigma_2(\tau) \rangle \propto f^2$ simply shifts vertically when f is changed. Figure 9 shows both the f -independent $\Sigma_2(\tau)$ (i.e., $f = 100\%$), and $\langle \Sigma_2(\tau) \rangle$ for natural Si ($f \sim 5\%$). Results are shown for magnetic field angles that yield the extremal slowest and fastest decoherence. For natural Si, in a wide range of τ about $\tau_{1/e}$, where $v_E(\tau_{1/e}) = 1/e$, $\langle \Sigma_2(\tau) \rangle$ matches $\tau^{2.3}$ curves very well. In this range of τ , therefore, we may write

$$v_E(\tau) \approx \exp(-f^2(\tau/\tau_0)^{2.3}) \quad (69)$$

$$= \exp(-(\tau/\tau_{1/e})^{2.3}), \quad (70)$$

where

$$\tau_{1/e} = \tau_0/f^{2/2.3} \propto f^{-0.87}, \quad (71)$$

providing a formula that allows us to adjust our Hahn echo curves to other values of f for a range of τ in which

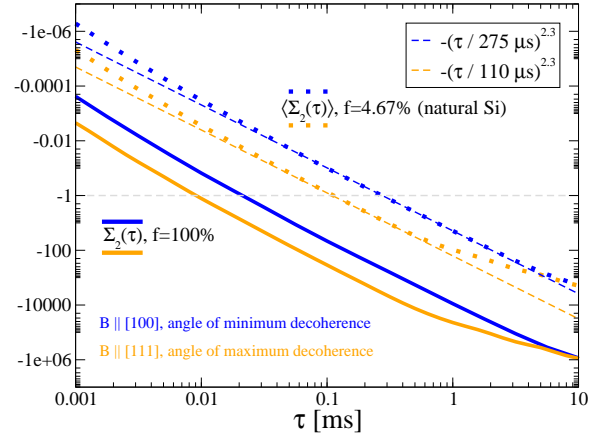


FIG. 9: Lowest order results for the natural log of the Hahn echo, $\ln(v_E(\tau)) \approx \langle \Sigma_2(\tau) \rangle \propto f^2$, for Si:P in a log-log plot. The solid lines give $\Sigma_2(\tau)$ with $f = 1$. Dotted lines give $\langle \Sigma_2(\tau) \rangle$ for natural Si ($f = 4.67\%$). In this log-log plot, multiplying by f^2 simply shifts the curves vertically. Isotopic purification would shift these curves up further. The two magnetic field angles shown give extremal results. Corresponding to θ angles in Fig. 8, $B \parallel [100]$ is $\theta = 0^\circ$ and $B \parallel [111]$ is $\theta \approx 54.7^\circ$. Dashed lines fit the natural Si curves near their -1 values (where $v_E \sim 1/e$) with $\tau^{2.3}$ power law curves (linear in the log-log plot).

Eq. (69) is applicable. Shortly after the original submission of this manuscript, experimental data from Abe *et al.* appeared in the literature³⁶ which shows echo time scaling ranging between $f^{-0.86}$ and $f^{-0.89}$, in remarkable agreement with our prediction [Eq. (71)]. Tyryshkin *et al.*¹⁰ report Si:P Hahn echo decay forms of $\exp(\tau^{2.4 \pm 0.1})$, in agreement with Eq. (69), with exception to magnetic field orientations near the [100] direction. In the [100] direction, they report a form of $\exp(\tau^{3.0 \pm 0.2})$; the reason for this discrepancy remains unknown.

We now check the convergence of our cluster expansion for this Si:P system. Using Eq. (41) and averaging over the isotopic configurations yields

$$\ln(v_E^{(k)}(\tau)) = \sum_{j=2}^k \langle \Sigma_j(\tau) \rangle + \mathcal{O}(\langle \Sigma^*(\tau) \rangle). \quad (72)$$

This approximates the ideal cluster expansion [see Secs. IV B 2 and IV B 3] with an error that we may estimate as $\langle \Sigma^*(\tau) \rangle = \langle \Sigma_2^*(\tau) \rangle + \langle \Sigma_3^*(\tau) \rangle$. This error is estimated by the correction needed to compensate for overlapping pairs [either the same pair overlapping itself, $\Sigma_2^*(\tau)$, or two different pairs overlapping, $\Sigma_3^*(\tau)$] in the approximation. Figure 10 shows these relative corrections, $\Sigma_2^*(\tau)/\Sigma_2(\tau)$ and $\Sigma_3^*(\tau)/\Sigma_2(\tau)$, to $\ln(v_E(\tau))$ for both $f = 100\%$ and natural Si ($f \sim 5\%$). The graphs also show the respective Hahn echoes (in a log time scale which alters their appearance) to show that these relative corrections are very small up to the tail of their respective echo decays. The argument, given in Sec. IV B 3, that $\Sigma^*(\tau)$ would be small was only applicable for $v_E(\tau) \gtrsim e^{-1}$

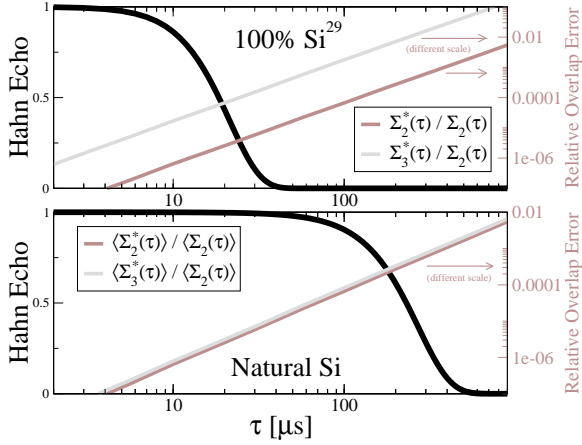


FIG. 10: Relative errors (with scales on the right) to the log of the Hahn echo due to overlapping pairs for both 100% ^{29}Si (top graph) and natural Si (bottom graph). In these examples, $B \parallel [100]$. The Hahn echoes themselves are shown, as well, with the 0 to 1 scales on the left. All curves share the same logarithmic time (τ) scale. It is apparent that these relative corrections are very small up to the tail of their respective echo decays.

so it is expected that this approximation approaches failure out in the tail of the decay. This is irrelevant for practical purposes.

The expansion of Eq. (72) is convergent where $\langle \Sigma_{k+1}(\tau) \rangle \ll \langle \Sigma_k(\tau) \rangle$ (implying that $\lambda L \ll 1$ effectively). The $\Sigma_k(\tau)$ functions have been calculated (up to $k = 5$) using Monte Carlo techniques with cluster contributions, $v_c^*(\tau)$, for clusters that are larger than pairs, calculated by numerically diagonalizing \mathcal{H}^\pm [Eq. (18)]. For each $\Sigma_k(\tau)$ independently, the maximum distance between neighbors and the maximum distance of nuclei to the donor is increased for various Monte Carlo runs until convergence within a desired precision is reached. To speed up each Monte Carlo run, clusters are chosen with a heuristic bias for those that have strong coupling between the constituent nuclei as well as a bias for clusters closer to the donor. Appropriate weighting factors are used to counteract these biases.

Figure 11 compares f -independent (i.e., $f = 100\%$) $\Sigma_k(\tau)$ functions in a dual (showing positive and negative values) log-log plot for Si:P with $B \parallel [100]$. In other words, it compares successive orders of the expansion for the natural log of the Hahn echo, $\ln(v_E(\tau))$, with the f dependence removed. As one might anticipate by the fact that $\Sigma_3(\tau)$ and $\Sigma_4(\tau)$ are both $\mathcal{O}(\lambda^4)$ (Sec. V proved that there are no odd orders of λ for either perturbation theory), they are similar orders of magnitude, at least for the $0.03 \text{ ms} < \tau < 1 \text{ ms}$ range. Near $\tau \sim 1 \text{ ms}$, however, the perturbation theory fails [having the condition that $\max(b_{nm})\tau \ll 1$] as we see that $|\Sigma_4(\tau)|$ surpasses $|\Sigma_3(\tau)|$. Interestingly, all orders approach the same order of magnitude near $\tau \sim 1 \text{ ms}$. We can thus identify the breakdown of the cluster expansion. Note, however, that this

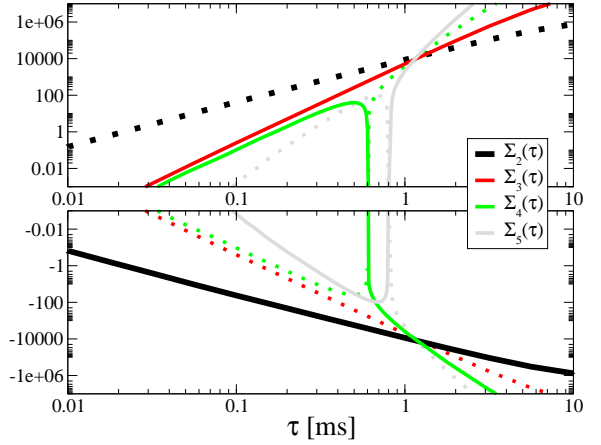


FIG. 11: Successive orders of the cluster expansion for the natural log of the Hahn echo [Eq. (72)], computed for Si:P and $B \parallel [100]$, for the 100% ^{29}Si theoretical scenario. The thick black line gives the lowest order result, $\Sigma_2(\tau)$, and other solid lines give higher order $\Sigma_k(\tau)$ results. The dotted lines give the negative of their corresponding functions provided to assist in the absolute value comparison of these higher order corrections. A failure of convergence occurs near $\tau \sim 1 \text{ ms}$ where all of the curves are the same order of magnitude. This occurs well into the tail of the decay, however, and therefore has no practical consequence.

is well into the tail of the decay [where $v_E(\tau) < e^{-1000}$] and therefore this breakdown is irrelevant for practical purposes. It is prudent, in any case, to understand the limitations of this expansion.

The $\langle \Sigma_k(\tau) \rangle$ curves for some fraction, f , of ^{29}Si will be the same as the $\Sigma_k(\tau)$ curves in the log-log plots of Fig. 11 except with appropriate vertical shifts [multiplying by f^k effectively appears as addition by $k \log(f)$ in the log plot] due to the f dependence. Higher orders will be shifted closer to zero than the lower order curves and therefore these curves will be more separated (actually improving the cluster expansion convergence). The top graph of Fig. 12 is analogous to the bottom (negative range) graph of Fig. 11 for natural Si (dashed lines indicate negated curves, i.e., where values are actually positive). We show only the low order corrections to the log of the Hahn echo, including $\langle \Sigma^*(\tau) \rangle$ as well as $\langle \Sigma_3(\tau) \rangle$ and $\langle \Sigma_4(\tau) \rangle$ and not bothering with $\langle \Sigma_5(\tau) \rangle$. $\langle \Sigma_3(\tau) \rangle$, with its inclusion of 3-cluster, gives the largest correction. Although $\Sigma^*(\tau)$ is of a comparable order of magnitude, its correction partially cancels the $\Sigma_3(\tau)$ correction because they are opposite in sign. We may therefore use $\Sigma_3(\tau)$ for a conservative estimate of the error of the lowest order cluster expansion result. The bottom graph of Fig. 12 shows the absolute (as opposed to relative) error of the lowest order Hahn echo result estimated by the inclusion of $\Sigma_3(\tau)$. The Hahn echo is displayed for reference. At its maximum, this absolute error is approximately 0.001. Although our cluster expansion fails near $\tau \sim 5 \text{ ms}$ [where $|\langle \Sigma_2(\tau) \rangle| \sim |\langle \Sigma^*(\tau) \rangle| \sim |\langle \Sigma_3(\tau) \rangle| \sim |\langle \Sigma_4(\tau) \rangle|$], the absolute error will stay small if we assume that our Hahn echo

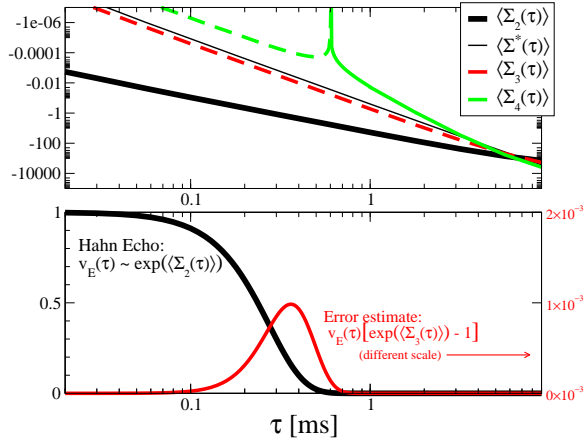


FIG. 12: Low order corrections to the Hahn echo, $v_E(\tau)$, computed for Si:P in natural Si ($f = 0.0467\%$) with $B \parallel [100]$. (top) Log-log plot of low order contributions to the natural log of the Hahn echo, $\ln(v_E(\tau))$. Ordinate axis is negative as in the bottom graph of Fig. 11; however, dashed lines indicate negated curves (and thus represent positive values). (bottom) Conservative estimate of the absolute error of the lowest order Hahn echo result (scale on the right) due to 3-cluster contributions, $\Sigma_3(\tau)$. The lowest order Hahn echo result is shown as a reference (scale on the left). The logarithmic time scale is the same for all plots (top and bottom).

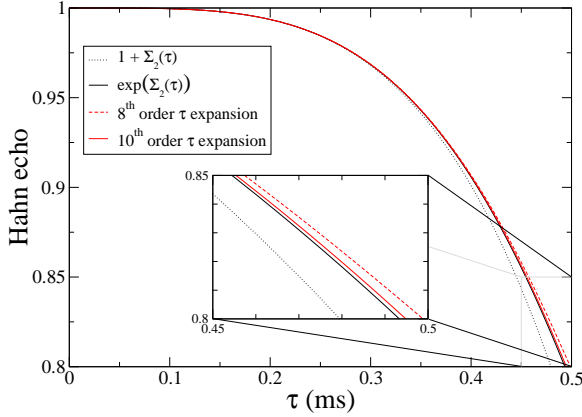


FIG. 13: This compares the τ -expansion results with the lowest order cluster-expansion result, $\exp[\Sigma_2(\tau)]$ [Eq. (32)], for an arbitrary set of nuclei (ranging from 15 to 20 lattice constants away from the center) for the phosphorus donor in natural silicon. Shown are the τ -expansion results at the highest two orders of τ that we have computed. Note the agreement with the cluster expansion results before the two τ -expansion results diverge. Also shown is $1 + \Sigma_2(\tau)$; its disagreement indicates the importance of accounting for simultaneous pairs in the cluster expansion.

decay is forever monotonically decreasing. For all practical purposes, the lowest order result is therefore valid up to 0.1% of the initial $v_E(0) = 1$, and higher order terms only provide corrections beyond 99.9% accuracy level.

We have also verified that our cluster expansion results agree quantitatively with the τ -expansion [Eq. (44)] (ap-

plied directly, not in the context of the cluster expansion) up to tenth order in τ when excluding nuclei close to the center of the electron wave function where $c_{nm} \gg 1$. This provides an independent verification of the cluster method approach. An example is given in Fig. 13. As discussed in Sec. V A, however, numerical calculations show that dipolar perturbation theory accounts for the Hahn echo decay in physically relevant systems we have studied. This is because clusters for which this perturbation theory is applicable will tend to operate on shorter time scales (due to the corresponding large hyperfine energies). This has been shown by comparing the lowest order cluster expansion using exact pair contributions versus approximate pair contributions in the lowest dipolar perturbation order as discussed in Sec. V A.

B. Gallium arsenide quantum dot

Next we consider the Hahn echo decay of a localized quantum dot electron spin in GaAs. For this, $\Psi(\mathbf{R}_n)$ will be the quantum dot wave function parameterized by the quantum well thickness, z_0 , and Fock-Darwin radius, $\ell(B)$ (a function of the magnetic field strength), as described in Ref. 9. Using this in Eq. (62), we have⁹

$$A_n = \frac{16}{3} \frac{\gamma_S \gamma_I \hbar (a_{\text{GaAs}}^3 / 4)}{\ell^2(B) z_0} d(I) \cos^2 \left(\frac{\pi}{z_0} Z_n \right) \times \exp \left(-\frac{X_n^2 + Y_n^2}{\ell^2(B)} \right) \Theta(z_0/2 - |Z_n|) - \gamma_S \gamma_I \hbar \frac{1 - 3 \cos^2 \theta_n}{|\mathbf{R}_n|^3} \Theta[X_n^2 + Y_n^2 - \ell^2(B)], \quad (73)$$

with $a_{\text{GaAs}} = 5.65 \text{ \AA}$ and $\gamma_S = 1.76 \times 10^7 (\text{s G})^{-1}$ (the free electron gyromagnetic ratio). The GaAs lattice has a zinc-blende structure with two isotopes of Ga atoms placed on one fcc lattice and ^{75}As atoms placed on the other fcc lattice.³² The Ga isotopes are 60.4% ^{69}Ga and 30.2% ^{71}Ga .^{9,37} We used $\gamma_I = 4.58, 8.16, 6.42 \times 10^3 (\text{s G})^{-1}$ and $d(I) = 9.8, 5.8, 5.8 \times 10^{25} \text{ cm}^{-3}$ for ^{75}As , ^{71}Ga , and ^{69}Ga , respectively.^{9,38} All of these nuclei have a valence spin of $I = 3/2$ which means that Eq. (67) is not applicable. Instead, cluster contributions are computed by numerically diagonalizing \mathcal{H}^\pm .

Most of our results only include dipolar interactions for b_{nm} [Eq. (9)]. However, indirect exchange interactions^{20,21,22} between the nuclei of GaAs may be of the same order of magnitude as the dipolar interactions [Eq. (9)] between nearest neighbors.¹³ There is enough quantitative ambiguity in the literature about the indirect exchange interaction that we have chosen to leave it out of our calculations in order to have a precise theory for the dipolar nuclear spin bath dynamics only. We make an exception near the end of this section where we make a comparison to the results in Ref. 13 that include this interaction.

With exception to the $I_{nz} I_{mz}$ term in \mathcal{H}^B [Eq. (8)], the different types of nuclei are decoupled. In the low-

est order of the cluster expansion, the different types of nuclei truly are decoupled because a pair cannot contribute to the spectral diffusion without the flip-flop interaction between them. Furthermore, this $b_{nm}I_{nz}I_{mz}$ term is negligible where the dipolar perturbation is applicable because the diagonal of the Hamiltonian in the nuclear z -basis will be dominated by \mathcal{H}^A . We will later discuss comparisons made between calculations using exact pair contributions versus approximate pair contributions using the lowest order dipolar perturbation (also done in Sec. VIA for Si:P) to demonstrate that the dipolar perturbation theory is applicable. Using these arguments, we will simplify our calculations by approximating Eq. (8) with

$$\mathcal{H}^B \approx \sum_{n \neq m} b_{nm} \delta(\gamma_n - \gamma_m) I_{n+} I_{m-}. \quad (74)$$

This approximation effectively decouples the As nuclei from the Ga nuclei and the Ga isotopes from each other. Although it is possible to perform our cluster calculations without this approximation (we have done so for some lowest order calculations with no additional complication and the difference is indeed negligible), it avoids unnecessary complications for higher order calculations. We may then perform calculations for each of these nuclear isotopes separately. Using the subscript x to represent each of these types of nuclei, the contributions to the natural log of the Hahn echo become

$$\langle \Sigma_k(\tau) \rangle = \sum_x f_x^2 \Sigma_{kx}(\tau), \quad (75)$$

$$\langle \Sigma_k^*(\tau) \rangle = \sum_x f_x^2 \Sigma_{kx}^*(\tau), \quad (76)$$

where $\Sigma_{kx}(\tau)$, $\Sigma_{2x}^*(\tau)$, and $\Sigma_{3x}^*(\tau)$ [Eqs. (37), (38), and (39), respectively] sum over clusters in the appropriate sublattice of isotope x , and f_x is the fraction of this isotope in its sublattice. For ^{75}As , ^{71}Ga , and ^{69}Ga , it is appropriate to use $f_x = 100\%$, 30.2% , and 60.4% , respectively. Monte Carlo techniques (described in Sec. VIA) are used to approximate these sums.

The lowest order results, $v_E(\tau) \approx \exp[\langle \Sigma_2(\tau) \rangle]$, for most of our GaAs calculations show a Hahn echo decay of the form $\exp[-(2\tau/t_0)^4]$. This differs qualitatively from the decay for the Si:P which, by our calculations, is in the form $\exp[-(2\tau/t_0)^\alpha]$ where $\alpha \sim 2.3$ for a range of τ appropriate for natural Si and some range of isotopic purification. The form of the GaAs echo decay does not change if we repeat the calculation with $I = 1/2$ rather than $3/2$, although t_0 does change. The qualitative difference between Si:P and GaAs dot solutions is therefore not due to the difference in spin magnitude of the nuclei, but rather the difference in the form of the electron wave function and lattice occupation leading to different distributions of c_{nm} values. GaAs, in ranges of tested z_0 and ℓ parameters, has a more narrow distribution of c_{nm} for significantly contributing pairs than that of the Si:P problem. As a result of this narrow distribution, the

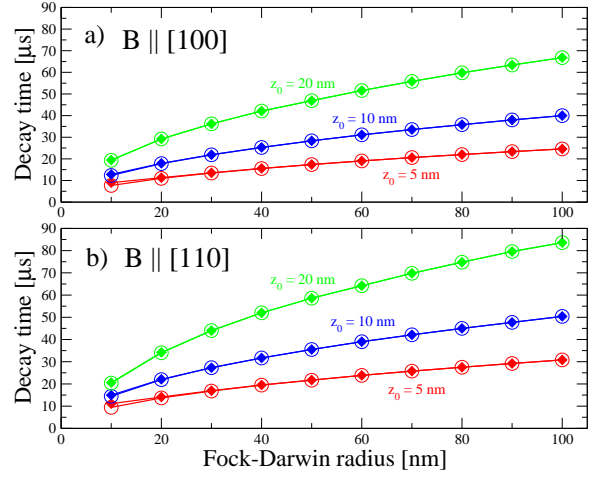


FIG. 14: For GaAs quantum dots, t_0 (circles), the characteristic initial decay time, and $t_{1/e}$ (diamonds), the e^{-1} decay time, vs the Fock-Darwin radius ℓ for various quantum well thicknesses, $z_0 = 5, 10,$ and 20 nm. The orientation of the magnetic field is (a) along the z_0 confinement of the quantum dot and $[100]$ lattice direction, and (b) perpendicular to the z_0 confinement direction and along $[110]$ of the lattice.

fact that the lowest nontrivial order of the τ -expansion is $\mathcal{O}(\tau^4)$, which is universal for all values of I , expresses itself in the sum of pair contributions in $\Sigma_2(\tau)$ [Eq. (37)]. This $\exp[-(2\tau/t_0)^4]$ form is confirmed by Yao *et al.*¹³ using a completely different theoretical technique. Yao *et al.* use a pair-correlation quasiparticle approach to the “spectral diffusion” problem that is equivalent to our lowest order cluster expansion, and they give results for quantum dots in GaAs. They come to the same conclusion that the form of the decay depends on the relative breadth of the excitation spectrum.

Figure 14 shows the t_0 of the initial $\exp[-(2\tau/t_0)^4]$ Hahn echo decay for various parameter settings of z_0 and ℓ with two different magnetic field orientations. Also shown is $t_{1/e}$, defined such that $v_E(\tau = t_{1/e}/2) = e^{-1}$. One can think of this $t_{1/e}$ as an effective T_2 -time for the problem although the echo decay is not a simple exponential. Except for small dots, $t_0 = t_{1/e}$, indicating that the decay has the form $\exp[-(2\tau/\tau_0)^4]$. Small dots deviate from this form, beginning to have longer $t_{1/e}$ decay times than their initial characteristic times, t_0 . It was noted in Ref. 9 that decoherence times become infinite as the size of the quantum dot approaches zero or infinity with a minimum decoherence time at some finite size. The former is simply because the electron has no interaction with nuclei as the quantum dot size approaches zero, and the latter is because the nuclei all have the same coupling to the electron as the size becomes infinite. For $z_0 = 5$ nm we begin to approach this maximum decoherence (minimum $t_{1/e}$) near $\ell = 10$ nm, but only in the regime where $t_{1/e}$ deviates from t_0 .

As discussed previously, the Ga and the As nuclei, on separate fcc lattices, are decoupled by our approxima-

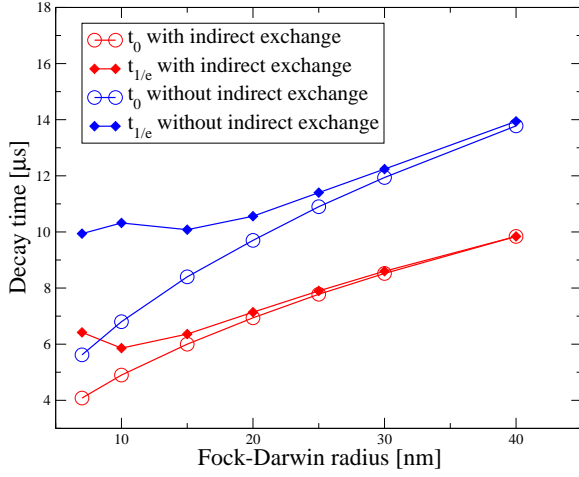


FIG. 15: For GaAs quantum dots, t_0 , the characteristic initial decay time, and $t_{1/e}$, the e^{-1} decay time, vs the Fock-Darwin radius ℓ for a quantum well thicknesses of $z_0 = 2.8$ nm. The orientation of the magnetic field is parallel to [110] of the lattice; this is perpendicular to the z_0 confinement of the quantum dot. This shows results both when including or excluding the indirect exchange coupling.

tion [Eq. (74)]. In silicon, the asymmetry of the diamond lattice results in maximum decoherence in the [111] direction. In this case, because the fcc lattice is more symmetric, the angular dependence is primarily a result of the shape of the quantum dot (not the lattice). Figure 14 shows slight quantitative differences when the magnetic field is along the z_0 confinement direction or perpendicular to it.

Because most of our GaAs results are in the form corresponding to the limit of small τ , it is tempting to think that GaAs is dominated by the $c_{nm} \ll 1$ regime appropriate for the τ -expansion. However, as with the phosphorus donor in Si, we have compared calculations that use exact pair contributions versus approximate pair contributions using the lowest order dipolar perturbation (also discussed in Sec. V A). These different calculations agree very well for small quantum dots, but deviate slightly for larger quantum dots. Intermediate sized dots are well-approximated by either perturbation theory. This is merely a result of small decoherence times such that the τ approximation is valid even though the dominating pairs have $c_{nm} > 1$. The agreement with the perturbation expansion gives justification for the approximation used in Eq. (74) in which $b_{nm}I_{nz}I_{mz}$ was neglected.

We now return to a discussion of the indirect exchange interaction between nuclear spins (mediated by virtual interband electronic transitions) that were neglected in the above calculations. Including the exchange interaction, we should use

$$b_{nm} = b_{nm}^d + b_{nm}^e, \quad (77)$$

where b_{nm}^d is the dipolar coupling [Eq. (9)], and b_{nm}^e is the indirect exchange coupling. We note that $b_{nm}^e = 0$ in the

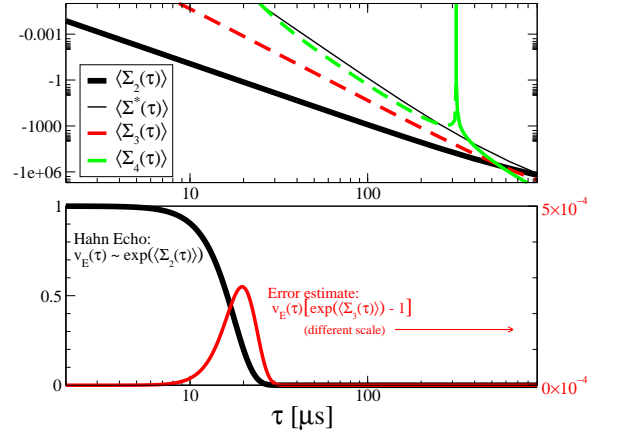


FIG. 16: Low order corrections to the Hahn echo, $v_E(\tau)$, computed for a GaAs quantum dot with $B \parallel [110]$, $z_0 = 10$ nm, and $\ell = 50$ nm. (top) Log-log plot of low order contributions to the natural log of the Hahn echo, $\ln(v_E(\tau))$. Ordinate axis is negative; however, dashed lines indicate negated curves (and thus represent positive values). (bottom) Conservative estimate of the absolute error of the lowest order Hahn echo result (scale on the right) due to 3-cluster contributions, $\langle \Sigma_3(\tau) \rangle$. The lowest order Hahn echo result is shown as a reference (scale on the left). The logarithmic time scale is the same for all plots (top and bottom).

Si:P system to a high degree of accuracy. Yao *et al.*¹³ performed spectral diffusion decoherence calculations (using an equation that is equivalent to our lowest order result) for GaAs quantum dots including the indirect exchange interaction. As a verification of the correctness of our calculations, Fig. 15 reproduces their Hahn echo results using our method but including the indirect exchange interactions as given by²²

$$b_{nm}^e = -\gamma_n \gamma_m \hbar \frac{\sqrt{2.6} \text{ \AA}}{2R_{nm}^4}. \quad (78)$$

There is ambiguity in the literature about the appropriate sign of Eq. (78). We have adopted the convention used by Yao *et al.*¹³ in order to reproduce their results. Figure 15 also shows the results for the same parameters when the indirect exchange is excluded; it is apparent that this coupling is significant, at least in GaAs quantum dots for these choices of the exchange coupling. The kink in the $t_{1/e}$ curve for the case of excluded indirect exchange is believed to be a discrete lattice effect only noticeable for small quantum dots. For such small quantum dots, it is likely that Eq. (73), derived from an approximate electron wave function, is somewhat inaccurate.

With our cluster expansion approach, we can estimate the error of our calculated decay curves by performing higher order calculations. We observe that the larger quantum dots have larger corrections. For quantum dots with $z_0 = 20$ nm and $\ell = 100$ nm our calculations indicate maximum correction to the Hahn echo decay curves on the order of 10^{-3} , 0.1% of the initial $v_E(0) = 1$, just as it was for natural silicon (Fig. 12). For dots with

$z_0 = 5$ nm and $\ell = 10$ nm, absolute corrections are on the order of 10^{-4} , 0.01% of the initial $v_E(0) = 1$. Fig. 16, analogous to Fig. 12, gives these low order corrections explicitly for an intermediate size ($z_0 = 10$ nm, $\ell = 50$ nm) GaAs quantum dot.

VII. CONCLUSION

In conclusion, we describe a quantum approach for the problem of localized electron spin decoherence due to the fluctuation of dipolar coupled nuclear spins. In contrast to former theories, our method requires no *ad hoc* stochastic assumption on the complex dynamics of the environment responsible for decoherence. Hence it provides an important example where direct integration of the environmental equations of motion provides a systematic understanding of the loss of coherence which needs to be controlled for quantum information applications.

The most important theoretical accomplishment of our work is the development of the first *fully quantum microscopic* theory for the localized electron spin decoherence due to the spectral diffusion induced by nuclear spin bath dynamics. The important nuclear spin dynamics for the spectral diffusion problem is the dipolar interaction induced nuclear spin flip-flops although for the GaAs quantum dot system, we have also included the indirect exchange interaction between the nuclear spins which turns out to be quantitatively comparable to the dipolar contribution to spectral diffusion. Our results are formally exact, and our numerical calculations provide an essentially exact (to better than 0.1% of the initial value) quantitative description of the Hahn spin echo decay. The significance of our quantum theory lies in the fact that, unlike all other theoretical descriptions of spectral diffusion spanning the last 50 years, we do not make any *ad hoc* phenomenological stochastic approximation in dealing with the non-Markovian spin dynamics in the spectral diffusion phenomena. We solve the problem essentially exactly using a quantum cluster decomposition technique, which is then theoretically justified by carrying out calculations to higher orders and by comparing with two independent perturbation techniques (i.e., the tau expansion and the dipolar perturbation theory). Very recently, a completely independent verification of our theory and results has appeared in the literature.¹³

Our theory for spin decoherence is restricted to understanding the so-called T_2 -decoherence of a single localized spin in a solid due to the dipolar nuclear spin flip-flops in the surrounding nuclear spin bath and in the specific context of a spin echo experiment. We neglect spin decoherence effects arising from the direct hyperfine coupling between the central spin and the surrounding nuclear spins, which would contribute to the free induction decay signal, but can be corrected by the spin echo technique. Our method uses a cluster expansion technique supported by two underlying perturbation theories: the dipolar perturbation expansion and the tau-expansion.

Each of these perturbation theories generates a unique expansion scheme in its own right, but only the cluster expansion converges for large systems [only for short times, $\tau \ll \max(b_{nm})^{-1}$, but often extending to the tail of the decoherence decay]. The convergence of this expansion has to be explicitly checked in each application, as we have done in this work. It is possible that an alternative more conventional perturbation theory for the non-Markovian spectral diffusion problem can be developed within the standard interaction picture of the many-body quantum theory which would be completely equivalent (for short times) to our cluster expansion technique. More work would be needed to clarify and establish such a possibility.

We note that spectral diffusion induced decoherence cannot be characterized by a simple T_2 time since the Hahn echo decay is not a simple exponential, and in fact, obeys different temporal power laws in the Si:P and the GaAs quantum dot systems. Spectral diffusion is a pure dephasing process arising from the temporal (non-Markovian) magnetic field fluctuations at the localized electron spin due to the nuclear spin dynamics, but it cannot be parameterized by a single T_2 time except as a crude approximation. Within this crude approximation, we find the spectral diffusion induced T_2 to be about 100 μ s for the Si:P system and about 10 μ s for the GaAs quantum dot system. But, this T_2 can be enhanced indefinitely (up to tens of milliseconds) in the Si:P system through the isotopic purification of Si (i.e., by removing ²⁹Si nuclei from the system) whereas in the GaAs quantum dots, $T_2 \sim 10$ μ s is essentially an absolute upper limit (when using simple Hahn echo refocusing) since *all* Ga and As nuclei isotopes have free spins contributing to the spectral diffusion and isotopic purification is impossible. It is important to emphasize here that although spin polarizing the nuclei (e.g., through the dynamic nuclear polarization technique) would, in principle, suppress the nuclear induced spectral diffusion decoherence of electron spin, in practice, this would lead only to rather small enhancement of electron spin coherence since the presence of even a few nuclei with the “wrong” spin would cause nuclear pair flip-flop processes.³⁹

Finally, we comment on the fact that the spectral diffusion process is quite a generic and general phenomenon in *any* spin decoherence problem with coupled spin dynamics (e.g. electron and nuclear spins, different types of nuclear spins, etc.) where the dynamics of one spin species has nontrivial (i.e., non-Markovian) temporal effects on the evolution of the spin dynamics of the other species. For example, a trivial (but not often emphasized in the literature) consequence of spectral diffusion consideration implies that in systems (e.g., Si:P; GaAs quantum dots) of interest to quantum computer architectures, the single flip of the localized electron spin will immediately decohere *all* the nuclear spins in its vicinity. Thus the nuclear spin T_2 time in these systems can at most be the T_1 time for the electron spin! The typical low-temperature T_1 time for electron spins in the GaAs

quantum dots has been measured to be 1 ms or so, and therefore the nucleus spin T_2 time would at most be 1 ms in the GaAs quantum dots, at least in the neighborhood of the localized electrons in the dot. The same consideration applies to the Si:P system. We believe that the general quantum theoretical techniques developed in this paper will be helpful in the studies of the temporal dynamics of other coupled spin systems wherever one spin species could act as a “decoherence bath” for the other system.

VIII. ACKNOWLEDGMENTS

We wish to thank Rogerio de Sousa, Eisuke Abe, Alexei Tyryshkin, Ren-Bao Liu, and most particularly Wang Yao for valuable correspondence and discussion. This work is supported by ARO-ARDA and LPS-NSA.

APPENDIX A: HAHN ECHO ANALYSIS

Here we derive Eq. (16) from Eq. (11) and related equations. By noting that

$$S_x + iS_y = S_+ = |1_e\rangle\langle 0_e|, \quad (\text{A1})$$

we may rewrite Eq. (11),

$$v_E(\tau) = 2 \text{Tr}_n(\langle 0_e|\rho(\tau)|1_e\rangle), \quad (\text{A2})$$

where the n subscript in Tr_n denotes a trace over the nuclear subspace. In addition to this equation, we will be referring to Eqs. (1)-(3), (5), and (8) for the free evolution Hamiltonian, $\mathcal{H} = \mathcal{H}^{Ze} + \mathcal{H}^{Zn} + \mathcal{H}^A + \mathcal{H}^B$, as well as Eqs. (12)-(15) to define the density matrix, $\rho(\tau)$, in terms of the evolution operator, $U(\tau)$, and initial density matrix, $\rho_0(\tau)$.

First we note that \mathcal{H}^{Ze} commutes with the rest of the Hamiltonian and that \mathcal{H}^{Zn} commutes with \mathcal{H}^A (since an operator commutes with itself and any operator that acts on an orthogonal state space). \mathcal{H}^{Zn} also commutes with \mathcal{H}^B (and therefore commutes with the entire Hamiltonian). This is proven by noting that \mathcal{H}^B preserves the overall polarization of like nuclear spins. That is,

$$[\gamma_n I_{nz} + \gamma_m I_{mz}, \delta(\gamma_n - \gamma_m) I_{n+} I_{m-}] = 0. \quad (\text{A3})$$

Let us define

$$U_0(t) = e^{-i\mathcal{H}t}, \quad (\text{A4})$$

and exploit the above commutation relations to write

$$U_0(t) = e^{-i\mathcal{H}^{Zn}t} e^{-i\mathcal{H}^{Ze}t} U'_0(t), \quad (\text{A5})$$

$$U'_0(t) = e^{-i(\mathcal{H}^A + \mathcal{H}^B)t}. \quad (\text{A6})$$

Using

$$\{\sigma_{x,e}, S_z\} = 0 \Rightarrow \sigma_{x,e} e^{-i\mathcal{H}^{Ze}\tau} = e^{i\mathcal{H}^{Ze}\tau} \sigma_{x,e}, \quad (\text{A7})$$

and the fact that \mathcal{H}^{Zn} commutes with $\sigma_{x,e}$ (the former acting only on the nuclear spins and the latter acting on the electron spin), we can rewrite Eq. (13)

$$U(\tau) = U_0(\tau) \sigma_{x,e} U_0(\tau) \quad (\text{A8})$$

$$= U'_0(\tau) \sigma_{x,e} U'_0(\tau) e^{-i\mathcal{H}^{Zn}(2\tau)} \quad (\text{A9})$$

$$= U'(\tau) e^{-i\mathcal{H}^{Zn}(2\tau)}, \quad (\text{A10})$$

$$U'(\tau) = U'_0(\tau) \sigma_{x,e} U'_0(\tau). \quad (\text{A11})$$

We can then rewrite Eq. (12)

$$\rho(\tau) = U'(\tau) e^{-i\mathcal{H}^{Zn}(2\tau)} \rho_0 e^{i\mathcal{H}^{Zn}(2\tau)} U'^{\dagger}(\tau) \quad (\text{A12})$$

$$= U'(\tau) \rho_0 U'^{\dagger}(\tau), \quad (\text{A13})$$

using the fact that \mathcal{H}^{Zn} commutes with ρ_0 (since it commutes with $|\chi_e^0\rangle\langle\chi_e^0|$, and $\mathcal{H}^n = \mathcal{H}^{Zn} + \mathcal{H}^B$).

At this point it is convenient, for clarity, to write our operators as block matrices in the electron spin z basis. First we have, from Eq. (A6)

$$U'_0(\tau) = \begin{bmatrix} U_+ & 0 \\ 0 & U_- \end{bmatrix}, \quad (\text{A14})$$

where

$$U_{\pm} = e^{-i\mathcal{H}^{\pm}\tau}; U_{\pm}^{\dagger} = e^{i\mathcal{H}^{\pm}\tau}, \quad (\text{A15})$$

with

$$\mathcal{H}^{\pm} = \mathcal{H}^B \pm \mathcal{H}^{An}, \quad (\text{A16})$$

$$\mathcal{H}^{An} = \frac{1}{2} \sum_n A_n I_{nz}. \quad (\text{A17})$$

U_{\pm} can be interpreted as the evolution operators of the nuclei with the electron spin constrained to be up or down, respectively, and ignoring the external magnetic field. Although U_+ and U_- are functions of τ , we have dropped this as an explicit parameter for convenience.

In this same electron spin basis, we can write

$$|\chi_e^0\rangle\langle\chi_e^0| = \frac{1}{2} \begin{bmatrix} 1 & e^{i\phi} \\ e^{-i\phi} & 1 \end{bmatrix}, \quad \sigma_{x,e} = \begin{bmatrix} 0 & 1 \\ 1 & 0 \end{bmatrix}, \quad (\text{A18})$$

in order to obtain, from Eqs. (14), (A13), (A11), and (A14),

$$\langle 0_e|\rho(\tau)|1_e\rangle = \frac{e^{i\phi}}{2M} U_- U_+ e^{-\mathcal{H}^n/T} U_-^{\dagger} U_+^{\dagger}. \quad (\text{A19})$$

Plugging this into Eq. (A2) gives

$$v_E(\tau) = \frac{e^{i\phi}}{M} \text{Tr} \left\{ U_- U_+ e^{-\mathcal{H}^n/k_B T} U_-^{\dagger} U_+^{\dagger} \right\}. \quad (\text{A20})$$

We are interested in the echo envelope which is given by the magnitude of Eq. (A20) and thus the $e^{i\phi}$ phase factor may be dropped.

APPENDIX B: INDEPENDENCE OF CLUSTER CONTRIBUTIONS

In order to prove the unique existence of the decomposition of $v_S(\tau)$ [the solution to the Hahn echo, $v_E(\tau)$, when only including the nuclei in some set \mathcal{S}] given by Eq. (20), we must prove that each cluster contribution is independent of anything outside of that cluster. Only then can we assume that the contribution of a given cluster is the same in every instance (i.e., in every term that involves this cluster) in such a decomposition.

Let us consider some cluster \mathcal{C} contained in \mathcal{S} . Because we are only concerned with the independence of processes in disjoint sets, let us remove any processes from $v_S(\tau)$ with coupling between nuclei in \mathcal{C} and nuclei in $\mathcal{S} - \mathcal{C}$. Define $v_{\mathcal{A}:\mathcal{B}}(\tau)$ to be the sum of all of the terms in the sum of products expansion (described at the beginning of Sec. IV B 1) of $v_{(\mathcal{A} \cup \mathcal{B})}(\tau)$ containing any factor of b_{nm} in which $n \in \mathcal{A}$ and $m \in \mathcal{B}$ (or vice versa). Thus, by definition, $v_S(\tau) - v_{\mathcal{C}:(\mathcal{S}-\mathcal{C})}(\tau)$ does *not* involve *any* coupling between a nucleus in \mathcal{C} and a nucleus in $\mathcal{S} - \mathcal{C}$; it only involves coupling amongst nuclei in \mathcal{C} or amongst nuclei in $\mathcal{S} - \mathcal{C}$. This is the same as calculating $v_S(\tau)$ if we artificially impose the condition that

$$b_{nm} = b_{mn} = 0 \quad \forall n \in \mathcal{C}, m \in \mathcal{S} - \mathcal{C}. \quad (\text{B1})$$

For convenience, we define the following:

$$V_S = U_{\mathcal{S}-} U_{\mathcal{S}+} U_{\mathcal{S}-}^\dagger U_{\mathcal{S}+}^\dagger, \quad (\text{B2})$$

$$U_{\mathcal{S}\pm} = e^{-i\mathcal{H}_{\mathcal{S}}^\pm \tau}, \quad (\text{B3})$$

$$\mathcal{H}_{\mathcal{S}}^\pm = \sum_{\substack{n \neq m \\ n, m \in \mathcal{S}}} \mathcal{H}_{nm}^B \pm \frac{1}{2} \sum_{n \in \mathcal{S}} A_n I_{nz}, \quad (\text{B4})$$

such that

$$v_S(\tau) = \frac{1}{M} \text{Tr} \{V_S\} = \frac{1}{M_S} \text{Tr}_{\mathcal{S}} \{V_S\}, \quad (\text{B5})$$

where M_S is the number of composite states for the nuclei in set \mathcal{S} and $\text{Tr}_{\mathcal{S}}$ takes the trace over only these states. Note that if we artificially impose condition (B1), then

$$\mathcal{H}_{\mathcal{S}}^\pm \rightarrow \mathcal{H}_{\mathcal{C}}^\pm + \mathcal{H}_{(\mathcal{S}-\mathcal{C})}^\pm. \quad (\text{B6})$$

Noting that $\mathcal{H}_{\mathcal{C}}^\pm$ commutes with $\mathcal{H}_{(\mathcal{S}-\mathcal{C})}^\pm$ (since they act on disjoint sets of nuclei), then

$$U_{\mathcal{S}\pm} \rightarrow e^{-i\mathcal{H}_{\mathcal{C}}^\pm \tau} e^{-i\mathcal{H}_{(\mathcal{S}-\mathcal{C})}^\pm \tau} \quad (\text{B7})$$

$$= U_{\mathcal{C}\pm} U_{(\mathcal{S}-\mathcal{C})\pm}, \quad (\text{B8})$$

$$V_S \rightarrow V_{\mathcal{C}} V_{(\mathcal{S}-\mathcal{C})}. \quad (\text{B9})$$

We may therefore write

$$v_S(\tau) - v_{\mathcal{C}:(\mathcal{S}-\mathcal{C})}(\tau) = \frac{1}{M_S} \text{Tr}_{\mathcal{S}} \{V_{\mathcal{C}} V_{(\mathcal{S}-\mathcal{C})}\} \quad (\text{B10})$$

$$= \frac{\text{Tr}_{\mathcal{C}} \{V_{\mathcal{C}}\} \text{Tr}_{(\mathcal{S}-\mathcal{C})} \{V_{(\mathcal{S}-\mathcal{C})}\}}{M_{\mathcal{C}} M_{(\mathcal{S}-\mathcal{C})}} \quad (\text{B11})$$

$$= v_{\mathcal{C}}(\tau) v_{(\mathcal{S}-\mathcal{C})}(\tau). \quad (\text{B12})$$

Equation (B11) is a direct consequence of the fact that $V_{\mathcal{C}}$ and $V_{(\mathcal{S}-\mathcal{C})}$ act on orthogonal subspaces of the Hilbert space because they act on disjoint sets of nuclei. We conclude that

$$v_S(\tau) = v_{\mathcal{C}}(\tau) v_{(\mathcal{S}-\mathcal{C})}(\tau) + v_{\mathcal{C}:(\mathcal{S}-\mathcal{C})}(\tau), \quad (\text{B13})$$

proving that processes involving disjoint sets of nuclei are independent for the following reason. Any interdependent process of cluster \mathcal{C} must be contained in the $v_{\mathcal{C}}(\tau)$ part of the right-hand side of Eq. (B13). This has no dependence on the set \mathcal{S} beyond the requirement that \mathcal{C} be contained in it. For this reason, the cluster contribution for cluster \mathcal{C} is well-defined in the sense that it is independent of all other nuclei.

We may also verify from Eq. (B13) that we are to multiply independent cluster contributions in order to account for simultaneous processes [the first term on the right side of Eq. (B13)] and that alternative combinations are to be included via addition (the second term). With this observation, we can decompose any $v_S(\tau)$ into a sum of products of cluster contributions. Recall that a cluster contribution includes all contributions from interdependent processes involving *only* and *all* of the nuclei in the cluster. Each process is thus assigned to only one cluster and there is no redundancy or overlap between different cluster contributions. Therefore, without redundancy, $v_S(\tau)$ is the sum of *all possible* products of cluster contributions as given by Eq. (20).

APPENDIX C: METHODS FOR COMPUTING THE ALGEBRAIC TAU-EXPANSION

We describe techniques used in our computer program for algebraically expanding Eq. (19) in orders of τ . For a particular order of τ , an expansion of the exponentials of $U_{\pm}(\tau)$ [Eq. (17)] will result in the trace of a sum of products of \mathcal{H}^\pm , and \mathcal{H}^B . The \mathcal{H}_{\pm} factors [Eq. (18)] can all be distributed to yield a sum of traces of products of \mathcal{H}^B , and $\mathcal{H}^{A_n} = \frac{1}{2} \sum_n A_n I_{nz}$. Each one of the Hamiltonian pieces, \mathcal{H}^{A_n} , and \mathcal{H}^B , involves sums over nuclear site indices. We can decrease the number of independent indices by one (not a major improvement, but enough to push this method one step further) by noting that

$$[\mathcal{H}^B, \mathcal{H}^{A_n}] = \frac{1}{2} \sum_{n \neq m} b_{nm} (A_n - A_m) I_n - I_{m+}, \quad (\text{C1})$$

which takes away the independence of \mathcal{H}^{A_n} 's index. Let $\mathcal{H}^C = [\mathcal{H}^B, \mathcal{H}^{A_n}]$. We can convert our sum of traced products of \mathcal{H}^{A_n} and \mathcal{H}^B into a sum of traced products of \mathcal{H}^{A_n} and \mathcal{H}^B and a single \mathcal{H}^C with one less independent summation index. The rest of this paragraph will briefly explain how this is done. Consider all of the terms that involve a certain number of \mathcal{H}^B 's and \mathcal{H}^{A_n} 's. For any term, we can permute the \mathcal{H}^{A_n} 's and \mathcal{H}^B 's however we want at the expense of creating terms in which an

$\mathcal{H}^B \mathcal{H}_{A_n}$ combination is replaced by \mathcal{H}^C (which is the type of term we want anyway). Consider the set of terms that all have a certain number of \mathcal{H}_{A_n} factors and a certain number of \mathcal{H}^B factors. As long as the coefficients of such a set add up to zero, we can make the permutations cancel out, leaving only the terms with \mathcal{H}^C and one less independent summation index. By the symmetry in $e^{\pm i \mathcal{H}^\pm \tau}$ of Eqs. (19) and (17), these coefficients add up to zero for all such sets in any order of τ .

Consider pulling the summations over nuclear site indices, not only outside of each product, but also outside of the trace (since the trace of a sum is equal to the sum of the traces). The trace of these spin operators involving particular nuclear sites is straightforward to compute. In fact, all one really needs to know to perform the trace is which indices are the same and which ones are different (as well as the magnitude of the nuclear spins). Then one can compute the trace as follows. If O_n is some operator (a product of spin operators I_{nz}, I_{n+}, I_{n-}) that operates on the spin of site n , then

$$\frac{1}{M} \text{Tr}(O_1 O_2 \dots O_k) = \frac{\text{Tr}(O_1)}{M_1} \frac{\text{Tr}(O_2)}{M_2} \dots \frac{\text{Tr}(O_k)}{M_k}, \quad (\text{C2})$$

where M_n is the number of states of the n^{th} spin. To compute $\text{Tr}(O_n) = \sum_i \langle i | O_n | i \rangle$ we simply use

$$\begin{aligned} I_\pm |I, m\rangle &= \sqrt{I(I+1) - m(m \pm 1)} |I, m \pm 1\rangle, \quad (\text{C3}) \\ I_z |I, m\rangle &= m |I, m\rangle. \quad (\text{C4}) \end{aligned}$$

Of course, in order to obtain an algebraic expression for a particular order of τ , we do not want to consider the sum of all possible nuclear site indices. In fact, in order to obtain this expression, we should not even need to know how many nuclear spins there are. Instead, we simply consider all of the possible ‘‘index configurations.’’ An ‘‘index configuration’’ indicates which indices are the same and which are different. As indicated above, this is enough information to allow one to evaluate the trace of the product of spin operators as a rational number [the square roots in Eq. (C3) will always be repeated as factors an even number of times in the trace]. Additionally, we need only consider ‘‘index configurations’’ that do not obviously result in a zero trace for any of the indices. In particular, we only need to consider configurations in which there are the same number of I_+ as I_- operators for each index, and we can ignore any configuration in which the only operator for any index is an odd power of I_z .

Once the operators and traces are taken care of and we have exhausted all ‘‘index configurations,’’ we are left with terms that have factors of A_n 's and b_{nm} 's, some with the same nuclear index labels, and some with different labels. These labels are to be summed over distinctly (i.e., different labels should never be assigned the same index). The labels are arbitrary, so when checking for ‘‘like’’ terms, in order to provide a compact expression for the result, we should consider that the labels can be

permuted. It would be a waste of computation time to always run through all permutations of labels when checking to see if two terms are like terms. Instead, the problem is transformed into that of checking for graph isomorphisms, which is a well-studied computational problem. The program uses a code called Nauty written by Brendan McKay (<http://cs.anu.edu.au/people/bdm>) for checking for graph isomorphisms.

The A_n and b_{nm} factors are transformed into a graph in the following way. Each distinct label is represented by a vertex in the graph. A factor of A_i^p is represented by coloring the vertex i to indicate the power p . A factor of b_{ij} is represented by an edge from vertex i to vertex j . If b_{ij} is raised to some power (other than 1) then it is represented by making an edge from both i and j to some special vertex that is colored in such a way as to indicate that it represents the appropriate power of b_{ij} (this is just a trick to effectively ‘‘color’’ edges). Then the Nauty program takes this graph and gives a canonical labeling for the vertices. If the program comes to another term of A_n and b_{nm} factors that are equivalent to this one up to a permutation of labels, Nauty will give it the same canonical labeling so that the two terms can be combined.

APPENDIX D: COMPUTATION OF TAU-EXPANSION COEFFICIENTS

Given an algebraic expression for a particular order, in τ , of $v_E(\tau)$, using the procedure described in Appendix C, we need to compute numerical coefficients for specific applications (with explicit values of A_n and b_{nm}). For a problem that has N nontrivial nuclei and an algebraic expression that has m terms and k summation labels, this will in general take $\mathcal{O}(mN^k)$ time to compute. This is a huge improvement over direct methods of evolving the state or diagonalizing the Hamiltonian since there are $\mathcal{O}[M = (2I + 1)^N]$ states of the system. So this expansion already saves us from calculations that grow exponentially with N . However, when N is on the order of 1000, which is actually a low estimate for considered applications, and we want the $\mathcal{O}(\tau^{10})$ term which has $k = 5$, N^k is still quite large (10^{15}). The situation can be drastically improved once more if we are willing to make another approximation which is very reasonable. We can set a threshold for values of $|b_{nm}|$, taking any $|b_{nm}|$ below this threshold to be zero. Since $|b_{nm}|$ generally decreases as nuclei are further separated, this amounts to a near neighbor approximation (also exploited by our cluster method). We can then adjust this threshold until convergence is achieved.

Let us say that our threshold is set such that, on average, each nuclei couples to L other nuclei. If we assume that all of the terms of the expression to be calculated are connected, not disjoint, graphs when representing labels as vertices and factors of b_{nm} as edges (as discussed in Appendix D in the context of checking for like terms), then this approximation reduces the computation time

to $\mathcal{O}(mNL^{k-1})$. For the first label, there are N possible nuclei to which it can be assigned, but each additional label must be one of the $\mathcal{O}(L)$ vertices connected by an edge to a previous vertex/label.

Not all of the terms, in general, have these connected graph representations, however. Some of them are disjoint. This does not create a real problem though. These “disjoint” terms can be factored and dealt with separately. As a simple example,

$$\sum_{i,j,k,l}^{\text{distinct}} b_{ij}b_{kl} = \sum_{i \neq j} b_{ij} \sum_{k \neq l} b_{kl} - 2 \sum_{i \neq j} b_{ij}^2 - 4 \sum_{i,j,k}^{\text{distinct}} b_{ij}b_{jk}, \quad (\text{D1})$$

where the summation on the left (and one of them on the right) is over distinct indices as indicated above the summation symbol. The second term on the right has the factor of 2 because it includes $b_{ij}b_{ji} = b_{ij}^2$ (since $b_{nm} = b_{mn}$). The last term gets a factor of 2 from $b_{jk} = b_{kj}$ and another factor of 2 from

$$\sum_{i,j,k}^{\text{distinct}} b_{ij}b_{ik} = \sum_{i,j,k}^{\text{distinct}} b_{ji}b_{jk} = \sum_{i,j,k}^{\text{distinct}} b_{ij}b_{jk}, \quad (\text{D2})$$

in which we relabeled indices.

Our computer program, described in Sec. VB 1, automatically performs these conversions as a preprocess before being fed to the program that performs the numerical calculations. In addition to this conversion for “disjoint” terms, the preprocessor performs a simple unidirectionally cascading factorization, for example, of the form $a[c + d(e + f)]$ but not $(a + b)(c + d)$, which reduces the number of multiplications that must be performed in the calculation. This factorization does not change the time complexity of the calculation, which is $\mathcal{O}(mNL^{k-1})$, but it does provide a noticeable speedup.

APPENDIX E: DIPOLAR PERTURBATION AND CLUSTER SIZE

In this appendix we prove that the contribution of a cluster of size k is $\mathcal{O}(\lambda^k)$ with respect to the dipolar perturbation expansion of Sec. VC, at least when $\tau \ll \max(b_{nm})^{-1}$. A direct application of quantum perturbation theory to the Hahn echo yields Eq. (53), giving a sum of oscillations of amplitude $C_{ijkl} = F_{ijkl}/D_{ijkl}$ and frequency $\omega_{ijkl} = \omega_{ijkl}^{(0)} + \lambda\omega'_{ijkl}$.

First, let us only consider the nuclei involved in a term of F_{ijkl} (the numerator of C_{ijkl}). The way in which nuclei “get involved” in F_{ijkl} is via the sum over nuclear pairs in $\mathcal{H}' = \frac{1}{\lambda}\mathcal{H}^B$. This gives potentially two nuclei for one λ , but we need to do better than that. Substituting $|k_{\pm}\rangle$ on the right-hand side of Eq. (47) with the full expression will give successive orders of λ . When one considers a

particular term of $\langle l^0 | k_{\pm} \rangle$ with the above recursion formula in mind, one will go from state $|l^0\rangle$ to state $|k^0\rangle$ with some number of intermediate \mathcal{H}^0 eigenstates in between where each state is connected to the next via \mathcal{H}' . The second term in the numerator of Eq. (47) simply corresponds to going from state $|l^0\rangle$ to $|k^0\rangle$ through some number of intermediate states and then from $|k^0\rangle$ back to $|k^0\rangle$ through some more intermediate states. The point is simply that one goes from one state to a different state only via \mathcal{H}' [Eq. (18)]. With this in mind, Eq. (55) indicates that one must go from state $|i^0\rangle$ to $|j^0\rangle$ to $|k^0\rangle$ to $|l^0\rangle$ and back to state $|i^0\rangle$ with some number of states in between where consecutive states are connected via \mathcal{H}' . Because we must come back to state $|i^0\rangle$, for every lowering operator we pass through, we must also pass through a raising operator for the same spin. We now see that we cannot actually get two nuclei for one λ ; for each nucleus involved in a given term of F_{ijkl} , there is at least one order of λ .

The denominator, D_{ijkl} , works in a similar way, except that instead of one cycle from state $|i^0\rangle$ back to state $|i^0\rangle$, one has one of these going from $|i^0\rangle$ to $|i^0\rangle$, another going from $|j^0\rangle$ to $|j^0\rangle$, another going from $|k^0\rangle$ to $|k^0\rangle$, and another going from $|l^0\rangle$ to $|l^0\rangle$. But the result is the same; because these are all cyclic, there must be at least one order of λ for each nucleus involved. One then needs to perform the Taylor expansion of D_{ijkl}^{-1} . Let $g(\lambda) = D_{ijkl}(\lambda)$ and $f(\lambda) = \frac{1}{g(\lambda)}$. The Taylor series expansion is

$$f(\lambda) = \sum_{n=0}^{\infty} f^{(n)}(0) \frac{\lambda^n}{n!}, \quad (\text{E1})$$

where $f^{(n)}(\lambda)$ may be obtained recursively with

$$\left(\frac{g^{(m)}(\lambda)}{(g(\lambda))^k} \right)' = \frac{g^{(m+1)}(\lambda)}{(g(\lambda))^k} - k \frac{g^{(m)}(\lambda)}{(g(\lambda))^{k+1}}, \quad (\text{E2})$$

and then we note that $[g(0)]^k = 1$ so there will not be anything in the denominators of Eq. (E2) to worry about in the context of Eq. (E1). Examining the numerators in Eq. (E2), we note that for each derivative of $f(\lambda)$, we will lose at most one order of λ . But in Eq. (E1) for each derivative there is a factor of λ provided to compensate. If we write the λ expansion of $g(\lambda)$ as

$$g(\lambda) = \sum_{n=0}^{\infty} g_n \lambda^n, \quad (\text{E3})$$

then, when we make the transformation to $f(\lambda) = 1/g(\lambda)$, each instance of g_n will be accompanied by at least n orders of λ . Therefore, after Taylor expanding the inverse of D_{ijkl} , we preserve the property that there are at least as many orders of λ as the number of nuclei involved in a given term.

We have dealt with the numerator and denominator of the amplitude, but we must still consider the frequency.

We can rewrite the exponential in Eq. (53) as

$$e^{-i\omega_{ijkl}\tau} = e^{-i\omega_{ijkl}^{(0)}\tau} \exp(-i\lambda\omega'_{ijkl}\tau) \quad (\text{E4})$$

$$= e^{-i\omega_{ijkl}^{(0)}\tau} \sum_{n=0}^{\infty} \frac{(-i\lambda\omega'_{ijkl}\tau)^n}{n!}. \quad (\text{E5})$$

Thus we have transformed the perturbative part of the frequency into an amplitude (with a time dependence as well). We can now use a similar argument that was used for F_{ijkl} and D_{ijkl} . Each term of Eq. (59) will cycle from some state back to the same state with \mathcal{H}' connecting each intermediate state. As a result, there must be at least as many orders of λ in a given term of $\lambda\omega'_{ijkl}$ as there are nuclei involved. There will, however, be one extra b_{nm} -type factor without an accompanying $1/(A_n - A_m)$. This gets combined with τ and will be small as long as $\max(b_{nm})\tau \ll 1$. All of this can be exponentiated in the series of Eq. (E5), but that can only increase orders of λ without increasing the number of nuclei involved.

There is one final consideration. How many nuclei are involved in $\exp(-i\omega_{ijkl}^{(0)}\tau)$? From Eqs. (58) and (49), we see that this will include the nuclei that differ between states $|i^0\rangle$ and $|j^0\rangle$ along with the nuclei that differ be-

tween states $|k^0\rangle$ and $|l^0\rangle$. Since a term of F_{ijkl} will require linking state $|i^0\rangle$ to $|j^0\rangle$ to $|k^0\rangle$ to $|l^0\rangle$ and back to $|i^0\rangle$ via \mathcal{H}' (through some number of nuclear states), it must involve at least that many nuclei. So this factor will neither increase the number of involved nuclei nor change the number of λ factors.

We therefore conclude that, using an approximation that assumes $\max(b_{nm})\tau \ll 1$, there will be at least as many orders of λ in a term of the λ -expansion of Eq. (53) as there are nuclei involved. Therefore a cluster contribution of size k will be of $\mathcal{O}(\lambda^k)$ or a higher order of λ . This justifies the cluster expansion in the regime in which $c_{nm} \gg 1$ and $\max(b_{nm})\tau \ll 1$. To be more accurate and to relax the $\max(b_{nm})\tau \ll 1$ constraint, as long as $\max(b_{nm})\tau < 1$ we have shown that clusters of size k will give a contribution of order λ^{k-1} . Because it is consistent for different cluster sizes, k , and because clusters of size one do not contribute, this reduction by an order in λ does not have an impact upon the validity of the cluster expansion in any of its various forms (i.e., product form or exponentiated form). For simplicity of the discussion, however, we will regard $\max(b_{nm})\tau$ simply as another order of λ .

-
- ¹ B. Herzog and E.L. Hahn, Phys. Rev. **103**, 148 (1956); A.M. Portis, *ibid.* **104**, 584 (1956).
- ² G. Feher and E.A. Gere, Phys. Rev. **114**, 1245 (1959).
- ³ W.B. Mims and K. Nassau, Bull. Am. Phys. Soc. **5**, 419 (1960); W.B. Mims, K. Nassau, and J.D. McGee, Phys. Rev. **123**, 2059 (1961).
- ⁴ J.R. Klauder and P.W. Anderson, Phys. Rev. **125**, 912 (1962).
- ⁵ G.M. Zhidomirov and K.M. Salikhov, Sov. Phys. JETP **29**, 1037 (1969).
- ⁶ M. Chiba and A. Hirai, J. Phys. Soc. Jpn. **33**, 730 (1972).
- ⁷ B.E. Kane, Nature (London) **393**, 133 (1998).
- ⁸ D. Loss and D.P. DiVincenzo, Phys. Rev. A **57**, 120 (1998).
- ⁹ R. de Sousa and S. Das Sarma, Phys. Rev. B **68**, 115322 (2003).
- ¹⁰ A.M. Tyryshkin and S.A. Lyon (private communication); A.M. Tyryshkin, S.A. Lyon, A.V. Astashkin, and A.M. Raitsimring, Phys. Rev. B **68**, 193207 (2003); A.M. Tyryshkin, J.J.L. Morton, S.C. Benjamin, A. Ardavan, G.A.D. Briggs, J.W. Ager, S.A. Lyon, cond-mat/0512705.
- ¹¹ E. Abe, K.M. Itoh, J. Isoya and S. Yamasaki, Phys. Rev. B **70**, 033204 (2004); E. Abe, *et al.*
- ¹² W.M. Witzel, R. de Sousa, and S. Das Sarma, Phys. Rev. B **72**, 161306(R) (2005).
- ¹³ Wang Yao (private communication); Wang Yao, Ren-Bao Liu, and L. J. Sham, cond-mat/0508441.
- ¹⁴ R. de Sousa and S. Das Sarma, Phys. Rev. B **67**, 033301 (2003).
- ¹⁵ It is possible for virtual spin-flip transition between hyperfine-coupled electron and nuclear spins to produce an effective hyperfine-mediated interaction between distant nuclei. Although it can be suppressed by increasing the external magnetic field strength, it can be an important effect for free induction decay (Refs. 16 and 13); however, under the application of refocusing pulses, this leads only to a small visibility decay (Ref. 17).
- ¹⁶ C. Deng and X. Hu, cond-mat/0510379.
- ¹⁷ N. Shenvi, R. de Sousa, and K.B. Whaley, Phys. Rev. B **71**, 224411 (2005).
- ¹⁸ Our interest is in the “intrinsic” decoherence in the context of refocused spin echoes which is dominated by spectral diffusion. Free induction decay (without refocusing) is important during the duration of a single gate operation. Hyperfine-induced free induction decay has been recently studied in literature (Refs. 16,19).
- ¹⁹ D. Klauser, W.A. Coish, and D. Loss, cond-mat/0604252, Adv. Solid State Phys. (to be published).
- ²⁰ R.F. Shulman, B.J. Wyluda, and H.J. Hrostowski, Phys. Rev. **109**, 808 (1958).
- ²¹ N. Bloembergen and T.J. Rowland, Phys. Rev. **97**, 1679 (1955).
- ²² R.K. Sundfors, Phys. Rev. **185**, 458 (1969).
- ²³ J.R. Petta *et al.*, Science, **309**, 2180 (2005).
- ²⁴ E.L. Hahn, Phys. Rev. **80**, 580 (1950).
- ²⁵ J.M. Elzerman *et al.*, Nature (London) **430**, 431 (2004); M. Xiao *et al.*, *ibid.* **430**, 435 (2004); D. Rugar *et al.*, *ibid.* **430**, 329 (2004).
- ²⁶ R. de Sousa (unpublished).
- ²⁷ X. Hu, R. de Sousa, and S. Das Sarma, cond-mat/0108339 (2001).
- ²⁸ H.Y. Carr and E.M. Purcell, Phys. Rev. **94**, 630 (1954); S. Meiboom and D. Gill, Rev. Sci. Instrum. **29**, 6881 (1958).
- ²⁹ A.V. Khaetskii, D. Loss, and L. Glazman, Phys. Rev. Lett. **88**, 186802 (2002).

- ³⁰ W.A. Coish and D. Loss, Phys. Rev. B **70**, 195340 (2004).
- ³¹ C.P. Slichter, *Principles of Magnetic Resonance*, 3rd ed. (Springer-Verlag, Berlin, 1990).
- ³² C. Kittel, *Introduction to Solid State Physics*, 7th ed. (Wiley, New York, 1996).
- ³³ A. Abragam, *The Principles of Nuclear Magnetism* (Oxford University Press, London, 1961), Chap. IV, Eq. (63).
- ³⁴ S. Saikin and L. Fedichkin, Phys. Rev. B **67**, 161302(R) (2003).
- ³⁵ E. Yablonovitch *et al.*, Proc. IEEE **91**, 761 (2003).
- ³⁶ E. Abe, A. Fujimoto, J. Isoya, S. Yamasaki and K.M. Itoh, cond-mat/0512404.
- ³⁷ *CRC Handbook of Chemistry and Physics*, 70th ed., E-82 (CRC Press, Boca Raton, FL, 1989).
- ³⁸ D. Paget, G. Lampel, B. Sapoval, and V.I. Safarov, Phys. Rev. B **15**, 5780 (1977).
- ³⁹ S. Das Sarma, Rogerio de Sousa, Xuedong Hu and Belita Koiller, Solid State Commun. **133**, 737 (2005).